Aspergillus nidulans swoQ PLAYS AN IMPORTANT ROLE IN POLARIZED HYPHAL GROWTH

A Thesis

by

BRIGITTE BOMER

Submitted to the Office of Graduate and Professional Studies of
Texas A&M University
in partial fulfillment of the requirements for the degree of

MASTER OF SCIENCE

Chair of Committee,	Brian D. Shaw
Co-Chair of Committee,	Daniel J. Ebbole
Committee Member,	Xiaorong Lin
Head of Department,	Leland S. Pierson

December 2016

Major Subject: Plant Pathology

ABSTRACT

Filamentous fungi form polarized hyphae by concentrating the addition of new material at the apex of the cell. The mechanics of polarized hyphal growth are coordinated by the cytoskeleton which utilizes microtubules (MTs) and filamentous actin in order to facilitate vesicle trafficking. The cytoskeletal machinery implicated in the regulation of endocytosis and exocytosis during polarized growth is complex and has been studied extensively in recent years. Despite these efforts there are many gaps in the current growth model, and the exact role of the cytoskeleton on secretion and internalization mechanisms during polarized growth remains to be elucidated. In order to address this knowledge gap, this study investigates the contribution of cytoskeletal elements on polarized growth.

In this study, I identified the *Aspergillus nidulans* temperature-sensitive (TS) mutant, *swoQ*. A mutant allele in the *swoQ* gene results in abnormal polarity maintenance and cell morphogenesis in the *swoQ* strain, as evidenced by the presence of abnormally swollen cells. A forward genetic screen revealed the *swoQ* polarity defect was suppressed following transformation with the pRG3-47-1 library plasmid which encodes *myoA*, a class I myosin motor protein. A sub-clone of *myoA* was introduced into the *swoQ* mutant and wild-type which resulted in restoration of polarized growth in the polarity mutant and hyper-branching in both strains.

To further assess the influence of *swoQ*, the localization of various polarity markers including: FimA::GFP, Exo84::GFP, DnfA::GFP, and DnfB::GFP, were examined in the mutant strain. The localization of FimA::GFP and Exo84::GFP was abnormal in the *swoQ*

mutant. FimA is an actin nucleating protein which works alongside MyoA, an essential myosin in *A. nidulans*. Together these proteins facilitate the formation of actin patches which drive endocytosis. Here I show that overexpression of MyoA has a polarization effect on growing cells and is able to suppress the growth defect of the *swoQ* mutant.

DEDICATION

I dedicate this thesis to my mother and father who have supported me my entire life and inspired me to become a scientist, and my fiancé for his patience and love.

ACKNOWLEDGMENTS

I would like to thank my committee chair, Dr. Brian Shaw, and committee co-chair, Dr. Daniel J. Ebbole, and committee member, Dr. Xiaorong Lin, for their guidance and support throughout the course of this research. Their critical analysis of my work has made it much better than it would have been otherwise and have encouraged me to do the best research I can. The amount all of the people on my committee have taught me have and will help in my research endeavors.

Special thanks should be extended to my academic advisor, Dr. Brian Shaw, for giving me the opportunity to work with him over the last three years, including my time as an undergraduate researcher in his lab. His instruction in fungal cell biology has allowed me accomplish what I have in mycological research. His support of the work that I have done and as my development as a research cannot be understated.

Zach Schultzhaus has been a monumentally helpful labmate who has helped me constantly throughout my time in graduate school and has been a great friend. Also, I would like to extend thanks to two of my undergraduates that have worked under me, Jesse Gwinn and Nicole Donhauser for their assistance in my research and for the time they have spent helping me.

I am also indebted to Justin McCharen for his help in mutagenizing strains and screening for temperature-sensitivity. His work has been vital to the progression of my work.

CONTRIBUTORS AND FUNDING SOURCES

This work was supervised by a thesis committee consisting of Professors Dr. Brian D. Shaw and Dr. Daniel J. Ebbole of the Department of Plant Pathology and Microbiology (PLPM), Professor Xiaorong Lin of the Department of Biology. Of the members listed, Dr. Shaw is the academic advisor.

Multiple strains were provided by Zach Schultzhaus that were used in the completion of this research. The mutant collection used in this study was mutagenized and screened for temperature-sensitivity by Justin McCharen. A genomic library was provided by Greg May of the University of Texas Medical Branch.

All other work conducted for the thesis was completed by the student independently.

Graduate study was supported by Texas A&M University, the Louis Stokes Alliance for Minority Participation Bridge to the Doctorate fellowship program, and the National Science Foundation (NSF) though NSF Award No. HRD-1406755.

The contents of this work are solely the responsibility of the authors and do not necessarily represent the views of the National Science Foundation.

TABLE OF CONTENTS

Page

LIST OF FIGURES

Page

LIST OF TABLES

Page

CHAPTER I

INTRODUCTION

Cell polarity is a fundamental process necessary for growth and development in all cell types. Polarization allows for the cell to assemble specialized domains which facilitate complex developmental processes. These domains are spatially defined molecular cues which allow the cell to establish structural and molecular asymmetry at the cell surface. These cues generate sites at the plasma membrane (PM) which elicit the reorganization of the cell around these domains. Polarity plays a role in a variety of diverse processes such as differentiation, localized membrane growth, and directional cell migration (*1*).

The life cycle of filamentous fungi is dominated by apical extension, continuous growth at the tip of the cell (*2*). This group of fungi utilizes hyperpolarized cells, called hyphae (*3*). Hyphal filaments extend at the tip of the cell which allows the fungus to orient growth in response to environmental stimuli. This specialized ability is adapted to assist the organism in search of nutrients, causing invasive growth in tissue (*4*). Invasive hyphal growth is a requirement for colonization. Many fungi cause disease in humans or economically important crops by growing invasive hyphae. Therefore, mechanisms involved in fungal pathogenesis need to be understood in order to provide insight on disease control strategies and development of anti-fungal agents. Previous studies have only scratched the surface of understanding the mechanism of polarized growth in filamentous fungi.

The amenable genetics of *Aspergillus nidulans*, as well as the prevalence of apical extension, make it an ideal model for studying polar growth (*5*). Various genetic and biological studies in *A. nidulans* and other fungi attempted to develop a general outline to describe the molecular framework governing hyphal growth. In this model, the fusion of secretory vesicles at the hyphal tip has been shown to drive apical extension (*6-8*). Vesicles at the apex provide materials needed for tip growth and are centralized around a network of cytoskeletal elements which facilitate vesicle trafficking (*9*). The movement of these vesicles is facilitated by microtubules (MT) and filamentous actin (F-actin), which work alongside one another to facilitate endocytosis. Vesicles are trafficked to the tip by the cytoskeleton via motor proteins. These vesicles fuse with the cytoplasmic membrane and deliver their contents in order to expand the membrane (*10*). Contained within these vesicles are cell-wall remodeling enzymes (glucan synthases, chitin synthases, and endoglucanases) (*11*). The activity of these enzymes promote expansion at the apex by creating an area of increased cell-wall plasticity which allows for the addition of new membrane (*12, 13*).

Spitzenkörper

The vesicle supply center located at the tip of the cell is the center for polarized growth (*10*). This collection of vesicles in the apical dome of fungal hyphae make up a structure called the Spitzenkörper (SPK), named after the German word for "apical body" (*3*). The SPK is an intracellular structure associated with cytoskeleton and the endomembrane system, which coordinates growth directionality in filamentous fungi (*11*).

The SPK is comprised of an aggregation of large apical macrovesicles (70 to 90 nm in diameter) and small microvesicles (30 to 40 nm in diameter) (*10*). This collection of vesicles has been shown to be centralized around the actin cytoskeleton (*14*). More recently, the visualization of actin dynamics using Lifeact in *A. nidulans* allowed for the observation of two new structures centralized around the SPK and sites of F-actin polymerization (*15*). The apical actin array (AAA), is found just behind the tip, while the subapical web (SAW) is located greater than 15μm behind the endocytic collar (*15*). Previously, *A. nidulans* formin SepA, which polymerizes F-actin in growing hyphae, was found to localize at the apical dome, septa and a spot at the center of the SPK. (*16*). Together these data affirm that the dynamics of the SPK is centralized around this cytoskeletal matrix affirming the fact that actin elongates around the SPK and aids in the delivery of vesicles to the tip.

The vesicles have been shown to enclose a variety of cell-wall components needed for polarized tip expansion such as membranes, glycoproteins, and biosynthetic enzymes (*6, 17, 18*). For example, in *Neurospora crassa* chitin synthase Chs-1 is present in microvesicles which localize to the inner region of the SPK. In contrast, glucan synthase Gs-1 is present in macrovesicles which accumulate in the outer stratum of the SPK, encircling Chs-1 (*11, 19*). Additionally, type 2 P4-type ATPase phospholipid transporters (flippases), DnfA and DnfB, have been identified in *A. nidulans* (*20*). Flippases, like DnfA and DnfB, facilitate the movement of phospholipids between membrane leaflets and in *A. nidulans* have been shown to play a role in the asymmetrical distribution of the phospholipid phosphatidylserine at the tip. DnfA and DnfB display differential

localization and are likely complementary to the population of secretory vesicles in the SPK (*20*). DnfA was shown to localize to the apical PM in growing cells. While DnfB was shown to localize at a compact locus just behind the cell tip at the center of the DnfA apical structure. The differentiation between localization these flippases and vesicles are presumably related to the spatial control of cell-wall synthesis and hyphal extension (*20*).

In *Saccharomyces cerevisiae* sites of polarization have been shown to be directed by a protein complex called the polarisome (*21*). The yeast polarisome is responsible for microfilament formation at polarized growth sites, the organization of actin, and is responsible for linking cell polarity regulators such as Cdc42p to the cytoskeleton. Similar to the polarisome, the SPK has been shown to regulate microfilament organization (*12*). Yeast modules, Bud1 Ras-GTPase and Cdc42 Rho-GTPase, are conserved in filamentous fungi and have been shown to be responsible for the assembly of actin filaments and localization of other components to the apex of the cell during a polarization event in yeast (*22, 23*). Efforts to understand the polarisome in filamentous fungi has allowed fungal biologists to identify several yeast polarisome orthologs in *A. nidulans (21, 24)*. For example, the actin polymerizing protein, SepA, is an ortholog of the yeast protein Bni1which localizes at the SPK (*25*). This data and the identification of 16 polarisome orthologs in *A. nidulans* suggest that filamentous fungi utilize various polarisome-like components at the hyphal tip along with MTs and F-actin to organize the SPK (*17, 21*). Despite these analyses, it still remains unclear how a hypha establishes polarity and the full extent of the relationship between the SPK and the polarisome remains to be determined.

Endocytosis and exocytosis

The SPK is involved in hyphal morphogenesis and is able to control apical growth both spatially and temporally. As it moves along the apical dome the SPK is able to control the directionality and speed of polarized tip extension. This ability involves the recycling of proteins coordinated by secretion and internalization mechanisms at the tip of the cell. These processes allow fungi to rapidly rearrange the direction of their growth in response to external stimuli (*26, 27*). Exocytosis, a secretion mechanism implicated in membrane expansion in filamentous fungi, uses cytoskeletal elements to traffic secretory vesicles to the SPK. These vesicles are then distributed to specific sites along the PM where they fuse to deliver enzymes and material needed for cell-wall expansion (*28, 29*). The polarized transport of vesicles to the PM has been shown to be regulated by the Arp2/3 (Actin-patch-associated) complex (*30*) and exocyst complex (*31*). The Arp 2/3 complex, localized at the endocytic collar, regulates actin nucleation and stimulates polymerization; meanwhile, the exocyst complex is responsible for the tethering of secretory vesicles to the apical membrane (*32*). Counter to exocytosis, endocytosis is an internalization mechanism associated with nutritional uptake, recycling of the PM, and maintenance of hyphal shape (*33-35*). This mechanism uses several dozen proteins to target and form a coated vesicle to internalize molecules found at the PM. Soluble N-Ethylmaleimide-sensitive factor Attachment Receptor (SNARE) proteins facilitate vesicle docking at the Golgi where the fate of the vesicles is determined. The contents of these vesicles are either targeted for degraded or recycled back to the apex of the cell to be reused at the tip (*36*). In combination, these two highly complex processes employ numerous proteins and the

cytoskeleton to regulate membrane trafficking and hyphal growth in filamentous fungi.

The actin cytoskeleton

Together the actin and MT cytoskeleton are centralized at the tip ready to interact with the vesicle supply center to control tip growth. Secretion, membrane internalization mechanisms, and the cytoskeleton facilitate polarized membrane expansion and hyphal morphogenesis. Exocytosis relies on various cytoskeletal elements to ensure targeted secretion. This mechanism relies on the cytoskeleton to assist in the intracellular transport of vesicles and to overcome the energetic barrier for membrane fusion (*28, 29, 37*). The fungal cytoskeletal matrix is a dynamic structure comprised of thee polymers: F-actin, MTs, and septins (*38*). Together these structural polymers form a complex network of interlinking filaments and tubules which are capable of polymerizing and depolymerizing at different rates to drive filament dynamics. The varied functions of the cytoskeleton rely on the distinct mechanical properties of these polymers and the filaments they form. Three populations of actin exist in filamentous fungi, these are: patches, cables and rings. Actin patches are associated with sites of PM invagination and endocytosis (*39, 40*). These patches are located in the subapical collar have been shown to be associated with sites of endocytic uptake and various actin binding proteins, such as ARP-2/3 complex, fimbrin, and coronin (*35, 37, 41*). The role of the *A. nidulans* proteins actin, ActA, and fimbrin, FimA, in hyphal growth was examined by studying their localization *in vivo*. Both ActA::GFP and FimA::GFP have a similar localization in growing cells, and enriched in the subapical collar of growing hyphae and in septa in *A. nidulans* (*42*). This endocytic

collar can be seen in action in confocal videos of live hyphae tagged with Lifeact *(15)*. The subapical collar is a major site of endocytosis, which allows the recycling of various components needed for polarized growth in order to promote continuous growth (*20, 33, 35, 40, 42, 43*). Actin patches co-localize with various endocytic proteins, such as: Sac6, Sla2, Vrp1, Arc35, Rvs167 (*44-49*).

The growth and shrinkage of actin cables is controlled by a dynamic treadmilling process. This process simultaneously couples various rates of actin polymerization at the plus-end of the filament and disassembly actin monomers at the minus end. This property gives actin the ability to rapidly remodel itself in response to the cell's requirements at the time (*32*). The actin cables formed by treadmilling are found in the SPK and are anticipated to play a role in the delivery of secretory vesicles (*8, 18*).

Myosins are a class of actin-based motor proteins which rely on actin cables in order to facilitate the transport of proteins transporting different cargo (such as secretory vesicles and mRNAs) to sites of polarization (*33, 34*). These proteins rely on actin-activated hydrolysis of ATP by the myosin in order to move along actin cables. *A. nidulans* possesses four classes of myosins: class I, class II, class V, and the fungus-specific class XVII which contains a myosin motor head and a chitin synthase domain. In *A. nidulans* class II and V myosins were found to play a role in tip growth and septation. Class II, MyoB was found to localize to the septum as nodes or strings and deletion of this motor-protein led to cytokinesis defects or septation failure, lack of conidiation, extreme growth defects, and improper chitin deposition (*43*). While the Class V, MyoE appears as small puntae throughout the hyphae and at septa (*50-52*). MyoB and MyoE orthologs had a

similar role in *A. fumigatus* where a *ΔmyoB* leads to irregular accumulation of chitin and irregular septation, and *ΔmyoE* exhibited significant growth defects such as hyper-septation and a loss of hyphal polarity and conidiation (*53*).

Class I myosins, like *S. cerevisiae* Myo5, are characterized for their possession of a single heavy chain which like other myosins is made of a motor, neck and tail domain. The class I motor domain of this myosin contains both an ATPase site and an ATP-sensitive F-actin-binding site, while the neck domain binds to a single light chain, like calmodulin. An actin binding site found in the head, tail and membranes allow for this class of myosins to cross link actin filaments to membranes by the use of force generated by the actin-activated hydrolysis of ATP (*54*). This structure provides this class of motor proteins the ability to nucleate actin which facilitates the internalization of the endocytic vesicles. Myo5 has been shown to be present in endocytic patches during invagination (*55-58*). Class I myosins have also been shown to regulate actin nucleation via the Arp2/3 complex by interacting with: Las17p and Bbc1p (*48, 55, 59*).

The *N. crassa* class I motor protein, Myo-1 is a key component of the endocytic collar (*35*). Myo-1 is an actin nucleating factor which was shown to accumulate in cortical patches of the subapical collar. The Myo-1-GFP was shown to colocalize with other endocytic markers such as fimbrin and coronin, in a collection of small patches in the subapical collar. Deletion of *myo-1* in *N. crassa* resulted in distorted hyphal growth and disorganization of the actin cytoskeleton. This deletion caused a 95% reduction in growth and lacked aerial mycelia. The *Δmyo-1* mutant was unable to support a stable SPK which resulted in a disruption of normal exocytosis, resulting in hyphae with variable bulging

(*41*). Whereas the *myo-1* ortholog, *myoA* is essential in *A. nidulans* and cannot be studied using this approach (*60*). *A. nidulans* has a single class I myosin which has been shown to colocalize with actin-rich regions in the in cortex of hyphal tips (*61*). Examination of a conditionally lethal *myoA* mutant on repressing medium resulted in enlarged circular cells which showed reduced levels of secretion. These enlarged cells were incapable of hyphal extension and eventually died. The morphological alterations observed in the *myoA* further validate the critical role *myoA* plays in stability and function of the SPK in polarized growth and secretion (*60*).

Microtubule cytoskeleton

Various cytoskeletal elements have been studied for their role in endocytosis and exocytosis. Filamentous fungi utilize the cytoskeleton to regulate membrane trafficking and hyphal growth in filamentous fungi. For example, the long distance transport of vesicles toward the tip of the cell is facilitated by MTs. In *A. nidulans* GFP-α-tublin revealed that MTs are able to persist in a region in the tip of growing hyphae and (*62*).

Assembly of these MTs requires the presence of a MT organizing centers (MTOC). A MTOC is a major site of MT nucleation which provides directionality to the MT complex. These centers are primarily composed of γ-tubulin, a protein originally identified in *A. nidulans* which is conserved throughout eukaryotes (*63-65*). In higher eukaryotes γ-tubulin assembles into a 2.2-MDa ring complex comprised of 13 γ-tubulin subunits which associate with other proteins to form a γ-tubulin ring complex (γ-TuRCs) (*64*). This protein complex facilitates *de novo* formation of MTs by mimicking the plus-end allowing

α-tubulin and *β*-tubulin to bind (*64-66*). MTOCs have yet to be seen in hyphal tips and γ-tubulin has not yet been observed in *A. nidulans* despite numerous investigations. In a search for the origin of MT polymerization, KipA, a kinesin motor protein was used to track the plus-end of MTs. This investigation revealed MTs do polymerize at the tip and that GFP-KipA accumulates at MT plus-ends. The *ΔkipA* strain was also shown to loose directionality and grow in curves in the, due to a mislocalization of the SPK in the apex (*67*). KipA has been shown to be a part of the MT complex which directly interacts with LIS1 (*50*). Dynein is also a part of this complex along with the kinesin motor protein KipA. Dynesin has been shown to associated with the plus-end of this complex and has been shown to localize to the tip and moves toward the cell periphery as it grows (*68, 69*). Once dynein reaches the cortex of the cell it is activated and pulls the attached MT to the cortex of the cell. The Kip2 motor protein has been shown to be responsible for the localization of several proteins at the plus-end (*68*).

Rationale and significance

Despite the fact that many studies have examined the molecular components involved in apical extension it remains unclear how the cytoskeleton governs polarity establishment and tip growth in hyphae. The goal of this study was to use *A. nidulans* as a model to further examine the molecular toolkit used by hyphae to maintain directional growth. Previous studies which used forward genetic approaches to examine developmental mutants in *A. nidulans* were fruitful in identifying genes involved in polarity and similar investigations are likely to will reveal additional genes participating in polarized growth (*34, 70-76*). In order to identify proteins associated with the cytoskeleton this study examined a collection of temperature-sensitive (TS) mutant's defective in polarized hyphal growth. In this study, the *A. nidulans* developmental mutant *swoQ* was identified for its presence of abnormally swollen cells, and named after its "*swo*-llen" phenotype. The localization of various polarity markers, such as FimA, Exo84, DnfA and DnfB, revealed that *swoQ* plays an important role in the stability various endocytic and cytoskeletal components. It was also determined that overexpression of MyoA, an essential class I myosin in *A. nidulans*, has an epistatic effect on *swoQ* and was shown to restore polarized growth in this developmental mutant.

CHAPTER II

MATERIALS AND METHODS

Strains and culture conditions

All strains, plasmids, and primers used in this study are listed in Table 1, Table 2, and Table 3, respectively. In order to compare polarity phenotypes strains were cultured at 30^{o}C and at 42^{o}C, and grown on media as previously reported (*72, 77*). All reagents for media, buffer, and supplements were purchased from Sigma (St. Louis, MO, USA) unless otherwise indicated. Plasmids were amplified and maintained in *Escherichia coli* DH5α™ Competent Cells (Invitrogen, Carlsbad, CA, USA) using the manufacturer's protocol.

Table 1. Strains used in this study.

Strain	Genotype	Source
A773	*pyrG89;wA3;pyroA4*	FGSC*
A234	*pabaA1;yA2*	FGSC
A580	*biA1;wetA6*	FGSC
ASL91	*pyrG89; argB2; wA3; veA1*	FGSC
Asuw7	*biA1; wetA6; argB2; pyrG89*	This study
TsC-47	*swoQ*; *pyrG89; wA3; pyroA4; veA1*	This study
AB1	*swoQ*; *pyrG89; pc473-1:: pyrG^{Af}; wA3; pyroA4; veA1*	This study
AB2	*swoQ; pyrG89; myoA; pyrG^{Af}; wA3; pyroA4; veA1*	This study
AXB1	*swoQ*; *pyrG89; wA3; pabaA1; pyroA4; veA1*	This study
AXB4	*swoQ*; *pyrG89; fimA::GFP::argB; wA3; pyroA4; veA1?*	This study
AXB2	*swoQ*; *pyrG89; ΔnkuA::argB dnfB::gfp::pyrG; wA3; pyroA4; veA1*	This study
AXB3	*swoQ*; *pyrG89; ΔnkuA::argB dnfA::gfp::pyrG; wA3; pyroA4; veA1*	This study
AXL6	*swoQ*; *pyrG89; ΔnkuA::argB exo84::gfp::pyrG; pabaA1; wA3; pyroA4; veA1*	This study
ASUFG77	*fimA::GFP::argB; methG1; biA1; argB2; veA1*	(*42*)
ZSS2	*pyrG89; ΔnkuA::argB B::gfp::pyrG; pabaA1; pyroA4*	(*20*)
ZSS3	*pyrG89; ΔnkuA::argB dnfA::gfp::pyrG; pabaA1; pyroA4*	(*20*)
ZSS51	*pyrG89; ΔnkuA::argB; exo84::gfp::pyrG; pabaA1*	(*78*)

* Fungal Genetics Stock Center

Table 2. Plasmids used in this study.

Strain	Description	Source
pGEM-T easy vector	TA cloning vector for PCR product cloning	Promega
pGEM-*myoA*	*myoA* in pGEM-T easy vector	This study
pGEM-*swoQ-myoA*	*myoA* in pGEM-T easy vector	This study
pRG3-47-3-1	Library genomic insert containing *myoA*	This study
pRG3-AMA1-NotI	Multicopy autonomous plasmid; pyr-4	(*79*)
pRG3-AMA1 library	*A. nidulans* R153 genomic library	(*79*)

Table 3. Primers used in this study.

Primer	Sequence	Source
M13 Forward	5'- GTAAAACGACGGCCAGT -3'	(*34*)
RG3 Reverse	5'- GCATGCCTGCAGGTCGACTCT -3'	(*34*)
T7 promoter	5'- TAATACGACTCACTATAGGG -3'	Promega
SP6	5'- GATTTAGGTGACACTATAG -3'	Promega
MyoA +1kb up	5'- ACCAGTGTTGTAGGAGAG -3'	This study
MyoA +1kb down	5'- CAGCAGCGTCGAACTATAC -3'	This study
MyoA seq. P1	5'- TTC CTG TTT CTT GCG GTT TCT TTC -3'	This study
MyoA seq. P2	5'- ACCTGTGCTGTGTTCGGAC -3'	This study
MyoA seq. P3	5'- CGATGTGGCGGAGTTTCAAG -3'	This study
MyoA seq. P4	5'- AGGTTGTGTGTTCGTTGATTG -3'	This study
MyoA seq. P5	5'- CATTCGTCGGGCTGGTTTC -3'	This study
MyoA seq. P6	5'- GCGGAGAGGTTCTTGTTTCG -3'	This study
MyoA seq. P7	5'- CAGGACCGAAGAAAGCAAAGG -3'	This study
MyoA seq. P8	5'- TCGTTGATTGCCTCGTTGG -3'	This study
MyoA seq. P9	5'- TTGTCCCACCACTCTCGA -3'	This study
MyoA seq. P11	5'- GCTTGGGTGGTATTCAGTGG -3'	This study
MyoA seq. P12	5'- GCTGGTCCTTGTTCTTGTCTGTC -3'	This study
MyoA seq. P13	5'- CTGGATACGGATGGCACAC -3'	This study
MyoA seq. P14	5'- GCGAGTCAGGTATGGTATGGT -3'	This study

Mutagenesis and mutant screen

Strains examined in this study were selected from a previously generated *A. nidulans* TS UV mutant collection (*78*). This collection was screened for polarity defective mutants by replica plating strains at 30^{o}C and at 42^{o}C on fully supplemented minimal media. Strains of interest were then examined microscopically using methods previously described (*34*). The strain of interest, tsC-47, was identified in this screen and selected for its TS polarity defect as evidenced by the presence of abnormally swollen cells and uneven diameter hyphae. The mutation carried by tsC-47 was later defined as *swoQ,* and its role in polarization was assessed using standard protocols as previously described (*76*).

Growth experiments

Temperature-shift experiments

Growth experiments in this study were performed to evaluate polar growth. Temperature-shift experiments were conducted to further characterize polarity phenotype and assess whether polar growth can be recovered following a downshift or lost following an upshift. Mutant strains were grown on solid media with appropriate supplements then subjected to an upshift (from 30°C for 11 hours to 42°C for 5 hours) and a downshift (from 42°C for 11 hours to 30°C for 5 hours), followed by microscopic observation using methods previously described (*76*).

Conidia production assay

In order to examine if conidia production in the *swoQ* mutant was hindered, assays to quantify sporulation were performed as previously described (*80*). In this assay 10 µl of sterile water containing 10^6 spores were placed in the center of a solid plate of media and each strain was replica plated at both 30°C and 42°C for 5 days. Conidia were then collected with 2ml of sterile water and then quantified with a hemocytometer. These experiments were performed in triplicate.

Mating and genetic analysis of single gene mutation

Various experiments in this study utilized mating as a tool for genetic characterization and strain manipulation. All crosses in this study were performed using standard procedures on strain pairs containing reciprocal auxotrophic markers (*34, 77*). Since *A. nidulans* is haploid, a single gene mutation is expected to segregate 1:1 in crosses with wild-type. A sexual cross between *swoQ* (*pyrG89; wA3; pyroA4; veA1*) and wild-type strain A234 (*pabaA1; yA2*) was performed to determine if the mutant phenotype was found at a single locus.

The *wetA* mutation is commonly used as a standard genetic marker found on chromosome VII of *A. nidulans* FGSC A4 *(81)*. This marker and was selected because it was predicted to be linked to *myoA* on this chromosome. Both of these genes are found on the same side of the centromere on chromosome VII and because of this have a very small chance of recombination. The percentage recombination of the meiotic progeny in this cross were then analyzed in order to determine distance. The map distance between *swoQ*

to each marker was calculated as previously described (*34*). The *wetA* strain used in this study, Asuw7, was generated by crossing A580 to ASL91 (Table 1). Asuw7 was then crossed with *swoQ* mutant in order to determine the genetic linkage between the *wetA* and *swoQ* genes in relation to *myoA.* Ascospores from this cross were replica plated and grown on media with appropriate supplements in order to score genotypes. The *swoQ* mutant was also crossed with various WT strains in order to integrate various polarity markers such as: Exo84::GFP, Fimbrin::GFP, DnfA::GFP, DnfB::GFP.

Microscopic observations and imaging

Live-cell imaging techniques were used to visualize the spatiotemporal organization of proteins involved in polarization during hyphal growth. Germlings in this study were grown on solid minimal media with appropriate supplements. Microscopic observations were made as previously described and images captured with a Hamamatsu Flash Orca-ER cooled CCD camera (*34, 42, 82*). A detailed description of this imaging system was previously described (*34*). The imaging system used in this study was an Olympus BX51 microscope (Olympus America, Melville, NY, USA) outfitted with differential interference contrasts (DIC) optics and the Olympus DSU spinning disc confocal imaging system which will interface a Windows 7 based desktop using SlideBook™ (Version 5.0.0.1). Image and figures in this study were prepared using Adobe Photoshop CC 2014 version 14.2.

In order to visualize protein dynamics and localization *in vivo*, strains containing fluorescent markers were imaged using previously described live-cell imaging techniques

(*15*). Excitation wavelengths at 470 to 480 nm and emission wavelengths from 510 to 550 nm were used to visualize GFP. Olympus U-MNIBA2 filter cubes (Olympus America, Melville, NY, USA) were used alongside a specialized dichroic mirror in order to visualize of GFP. This dichroic mirror allowed for emitted light at the appropriate wavelength, 505 nm for GFP.

Transformation of *A. nidulans*

In order to identify the genes involved in polarization, the *swoQ* mutant was transformed with a genomic library, constructed in the autonomously replicating vector pRG3-AMA1-NotI (Table 2), as previously described (*54, 79*). The AMA1 sequence encoded in this vector allowed for extrachromosomal replication within transformants and increases transformation efficiency at least 100-fold to 1–2 X 10^4 transformants/µg DNA (*54, 83*). This property facilitates plasmid recovery and isolation of the plasmid responsible for restoring polarity to the *swoQ* mutant in subsequent steps. The pRG3-AMA1 genomic library (Table 2) used in this study was constructed using 20 genome equivalents of *A. nidulans* which were digested then ligated into the vector ranging from 6kb-20kb and averaging an insert size of 9kb (*54*). In order to transform *swoQ,* and in all transformations in this study, protoplasts were prepared and used as recipients of exogenous DNA previously described (*54, 79, 84*). All strains in this study are auxotrophic which allowed for the selection of prototrophic transformants as previously described (*77*). *swoQ* mutants were transformed with the genomic library and selected by assaying for restoration to *pyrG* prototrophy and restoration of the wild-type phenotype at 42ºC.

Plasmids were recovered from transformants which displayed the restored polarization phenotype. Recovered plasmids were then re-introduced into the *swoQ* mutant to confirm their ability to rescue the polarity defect.

Recovery of plasmids

The pRG3-AMA1 vector plasmid allows for autonomous replication, which facilitates plasmid recovery in subsequent cloning steps (*79*). Genomic DNA was isolated from *swoQ* transformants which displayed recovered polarity following transformation with the genomic library using standard protocols (*85*). DNA isolated from these transformants was then introduced into *E. coli* DH5α™ competent cells, using standard methods (*79*). Following transformation, bacteria containing the plasmid of interest were selected for based on ampicillin resistance encoded by the plasmid. The genomic insert found within isolated plasmids were presumed to be responsible for restoring polar growth of the *swoQ* mutant allele. To test this, recovered plasmids were then re-introduced into the *swoQ* mutant to re-confirm the rescued plasmid was responsible for the restoration to wild-type growth.

Sequencing and identification of *myoA* gene

Once the isolated plasmid was shown to restore wild-type growth in the mutant strain, the genomic insert of this plasmid was sequenced at the Texas A&M University Laboratory for Genome Technology (College Station, TX, USA). using inward facing primers previously described (*34*). These primers, M13 forward and RG3 reverse (Table

3) were designed specifically to the flanking region of the genomic insert contained in the pRG3-AMA1 vector (*34*). The flanking sequence obtained from this reaction was used to obtain the full sequence of the genomic insert. This data was analyzed using the Broad Institute *A. nidulans* genomic database (*58*) and then compared to the National Center for Biotechnology Information (NCBI) database (*59*) using Basic Local Alignment Search Tool (BLAST) (*86*).

Sequencing of AN1558 in tsC-47

The *A. nidulans* gene AN1558 along with 1kb both upstream and downstream was amplified through PCR using primers, MyoA +1kb up and MyoA +1kb down (Table 3). This PCR used Thermo Scientific® Phusion Flash High-Fidelity DNA Polymerase (Waltham, MA, USA) in order to amplify 6,079bp from tsC-47 genomic DNA. Following amplification of this gene was cloned into the pGEM®-T Easy Vector (Promega Corporation, Madison, WI, USA). The resulting plasmid was named pGEM-*swoQ-myoA,* and then sequenced by Eton Bioscience (San Diego, CA, USA) in order to determine if the AN1558 gene inside of the *swoQ* mutant possessed a mutation. The pGEM-*swoQ-myoA* plasmid was sequenced using 14 different insert specific primers (MyoA seq. P1 through 14), and two vector specific primers, T7 and SP6 (Table 3). These primers allowed for at least 2x coverage of the entire 6,079 bp fragment. Sequence data from this sequencing reaction was concatenated using Sequencher (Gene Codes Corporation, Ann Arbor, MI, USA) and compared against *A. nidulans* FGSC A4 AN1558 (AspGDID: ASPL0000043272) from the Aspergillus genome database.

Cloning and overexpression of AN1558

Sequence data identified the gene, AN1558. This gene was amplified with primers designed to amplify AN1558, MyoA Forward +1kb upstream and MyoA Reverse +1kb downstream (Table 3), using the A773 wild-type strain as template. This amplicon totaled 6,079 bp in size and was amplified through PCR with Thermo Scientific® Phusion High-Fidelity DNA Polymerase (Waltham, MA USA). Since *pfu* DNA polymerases produce blunt end products, the AN1558 amplicon was A-tailed using *Taq* DNA Polymerase (New England Biolabs, Ipswich, MA, USA) following amplification. The A-tailed PCR product was then ligated and cloned pGEM®-T Easy Vector (Promega Corporation, Madison, WI, USA) using manufacturer's protocols. The resulting plasmid, pGEM-*myoA*, was then used to transform both the *swoQ* mutant and A773 strain. This plasmid was transformed concurrently with the empty vector plasmid, pRG3-AMA1, in a co-transformation. As a control both the *swoQ* mutant and A773 strain were transformed only with the empty vector plasmid.

CHAPTER III

RESULTS

Identification of the *swoQ* mutant

In order to further the current understanding of invasive hyphal growth, this study utilized a forward genetic approach to identify genes involved in polarization. The tsC-47 strain was selected for this study from a collection of TS mutants because of its polarity phenotype at the restrictive temperature, 42ºC. In order to determine if the mutant allele found in tsC-47 occurs at a single locus, ascospores from an outcross between the tsC-47 and A773 strains were examined. *A. nidulans* is haploid, therefore a single gene mutation is expected to segregate 1:1 in crosses with wild-type. Progeny from this cross resulted in a mutant to wild-type segregation ratio of 94: 92 (n=186), where the *swo* mutation was found in 50.54 % of progeny. A chi-square (χ^2) goodness-of-fit test and a two-tailed test revealed that this result has a χ^2 of .022 with one degree of freedom, and a *p*-value of .8834. By conventional criteria and a level of significance where $\alpha = .05$, this difference is considered to not be statistically significant and does not differ significantly from the theoretical distribution. This result indicates the *swo* mutation segregates as one locus in the tsC-47 strain and because of this the mutation carried by this strain will referred to as *swoQ* hereafter.

The *swoQ* phenotype

The *swoQ* mutant was selected for this study because of its TS polarity phenotype. At the permissive temperature, 30ºC, this mutant grows as wild-type (Figure 1 and 2). While at the restrictive temperature, 42ºC, this strain displays a prominent TS polarity defect, as evidenced by the presence of abnormally swollen cells, uneven diameter hyphae, enlarged vacuoles, and an abnormal distribution of nuclei (Figure 1 and Figure 2). The hyphal diameter of this strain ranges from the typical 3 μm to 35 μm, where $\bar{x}$=15 μm and n=604 following a 12 hour incubation at 42ºC. Following an 11 hour incubation at the restrictive temperature, 44.4% of *swoQ* cells displayed the swollen cell polarity phenotype, 24.3% of cells grew as wild-type, and 31.3% did not germinate (n=304), in comparison A773 had 80.2% of cells germinate (n=258).

In order assess whether polar growth could be lost following a temperature shift, *swoQ* mutant cells were incubated for 11 hours at the 30ºC, then upshifted to the 42ºC for 5 hours. Following this incubation time, 40.2% of growing hyphae observed (n=250) lost polarization and began to swell apically (Figure 3). The remaining 32% of cells appeared as wild-type (Figure 3). In order to determine if polar growth can be recovered following a downshift in temperature, *swoQ* mutant cells were grown at 42ºC for 11 hours then transferred to 30ºC for 5 hours. Following this incubation protocol, it was observed that *swoQ* germlings were able to re-initiate polar growth resulting in multiple new sites of growth on each germling. *swoQ* germlings are able to establish multiple sites of growth, where 61% of cells have 3 to 4 polarization sites, 12% have 5 or greater, and the remaining 27% possessed 1 to 2 polarization sites (n=150) (Figure 4).

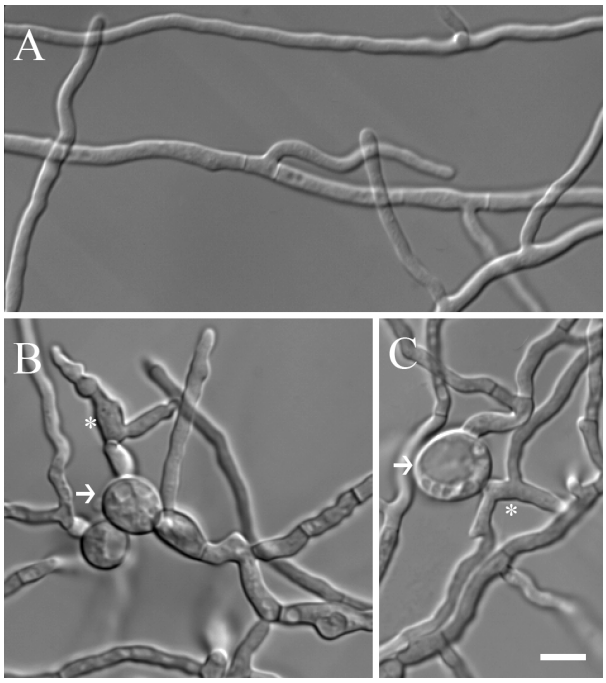

Figure 1. *swoQ* displays aberrant growth at the restrictive temperature.
TS mutant, *swoQ* displays a near normal phenotype at 30°C while at 42°C the mutant displays defective polarized growth. The *swoQ* mutant was grown for 12 hours at the restrictive temperature then imaged with DIC on agar blocks. (A) The *swoQ* strain grown at the permissive temperature. This temperature allows the mutant to develop a phenotype similar to WT and hyphae with a consistent diameter of 15 μm. (B, C) *swoQ* grown at the restrictive temperature causes the TS polarity defect to be displayed. At this temperature the mutant displays phenotypes such as swollen cells and uneven diameter hyphae, indicated by arrows and asterisks respectively. Scale bar=5μm.

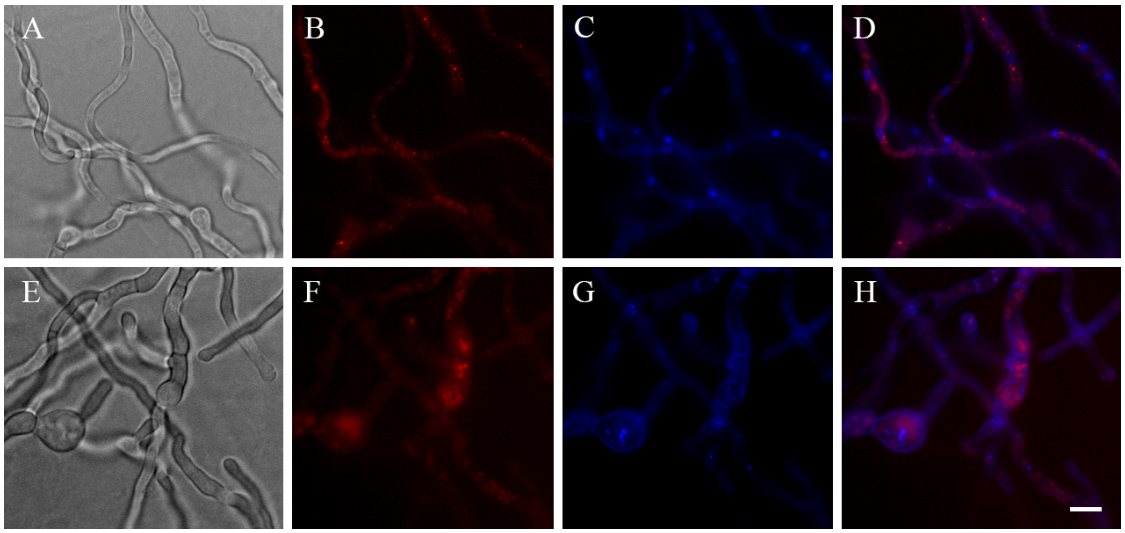

Figure 2. Mutant cells have an abnormal distribution of nuclei.
The *swoQ* mutant (E-H) phenotype displays an abnormal distribution of nuclei at 42ºC. Cells also have enlarged vacuoles (see also Fig. I) in comparison to WT (A-D) when grown at 42ºC for 16 hours. Cells were treated with FM4-64 and DAPI to visualize the PM and nuclei, respectively. (A, E) Bright-field, (B, F) FM4-64, (C, G) DAPI, (D, H) overlay. Scale bar=5 μm.

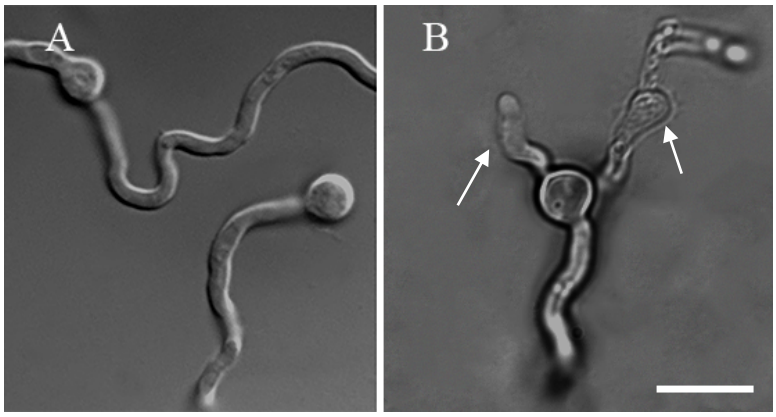

Figure 3. Polarized growth is lost following an upshift.
Polarized growth in the *swoQ* mutant is lost when shifted from the permissive temperature to the restrictive temperature. (A) The *swoQ* mutant was grown for 11 hours at 30ºC. (B) The *swoQ* mutant was grown for 11 hours at 30ºC then shifted to 42ºC for a 5 hour incubation. Polar growth is lost in 40.2% of upshifted *swoQ* strains. These strains loose polarization and begin to swell, as indicated by arrows. Scale bar =10 μm.

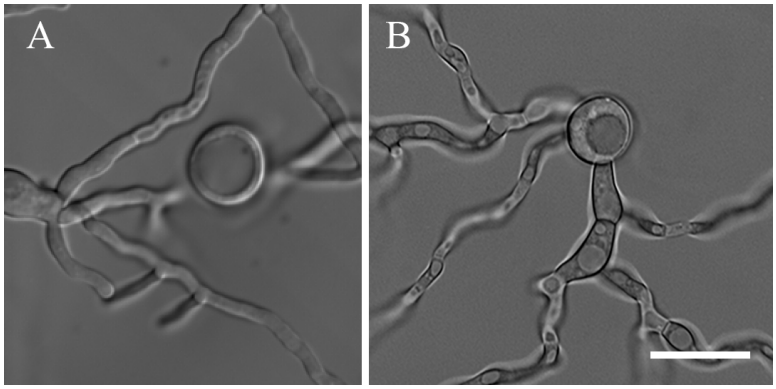

Figure 4. Multiple germ tubes emerge following a downshift.
Cells were grown at the restrictive temperature for 11 hours then shifted to the permissive temperature for 5 hour in order to determine if polarized growth can be restored. (A) The *swoQ* mutant was grown for 11 hours at 42ºC. (B) The *swoQ* mutant was grown for 11 hours at 42ºC then shifted to 42ºC for a 5 hours incubation. Scale bar=10 μm.

Polarized growth in *swoQ* mutant is restored by pRG3-47-1

The tsC-47 strain was transformed with the pRG3-AMA1 genomic library in order to identify a plasmid which contained a genomic insert capable of restoring polarized growth to *swoQ* (Table 2) . Transformants were screened for the restoration of wild-type like growth at the restrictive temperature and pyrimidine (*pyrG*) prototrophy on minimal medium. In this screen 1,400 prototrophic transformants were observed but only one transformant displayed wild-type like growth at the restrictive temperature. The library plasmid responsible for restoring polarized growth to the transformed *swoQ* strain was isolated by transforming competent bacterial cells with genomic DNA from the transformants of interest. Library plasmid pRG3-47-3-1 (Table 2) was recovered and re-introduced into the *swoQ* mutant which confirmed this plasmid restores growth to the *swoQ* mutant at 42°C (Figure 5).

The genomic insert of the rescued plasmid, pRG3-47-3-1, was sequenced using vector specific primers, M13 and RG3 (Table 3). Analysis of sequence data from this set of reactions revealed the location of the genomic insert in pRG3-47-3-1 was not found in the MCS as anticipated, but rather located inside of pyr4, this result is further detailed in Figure 6, due to an as yet uncharacterized recombination event with in the plasmid. The full sequence of the genomic insert was obtained by comparing pRG3-47-3-1 sequence data to the NCBI database using blastn (*86*). End sequence belonging to the genomic insert of pRG3-47-3-1 was shown to possess 1,058 nucleotides of coding sequencing belonging to *myoA* (AN1558), a putative myosin I required for secretion and polarized growth (Figure 6).

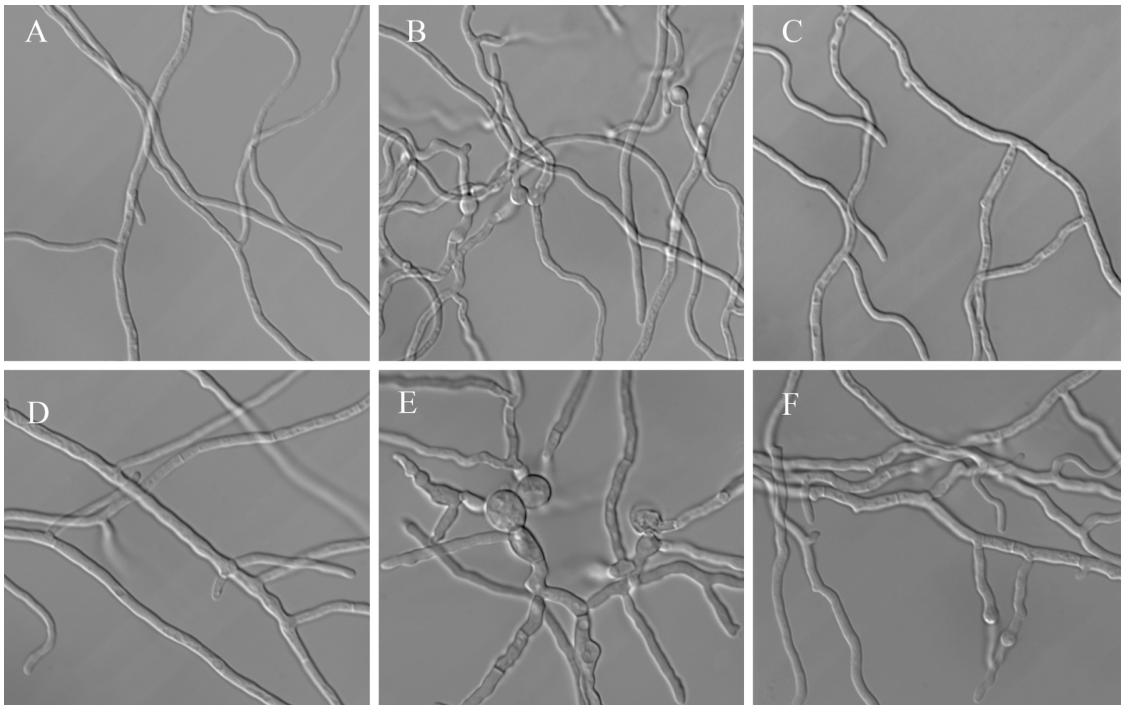

Figure 5. pRG347-3-1 restores polarized growth to *swoQ* transformants.
The genomic library plasmid, pRG3-47-3-1, rescues the *swoQ* mutant phenotype. To evaluate differential growth between the permissive (A-C) and the restrictive (D-E) temperatures, strains were grown at their respective temperature for 16 hours, then imaged with DIC on agar blocks. (A, D) WT, (B, E) *swoQ* mutant, (C, F) *swoQ* strain transformed with pRG3-47-3-1. Scale bar=5 µm.

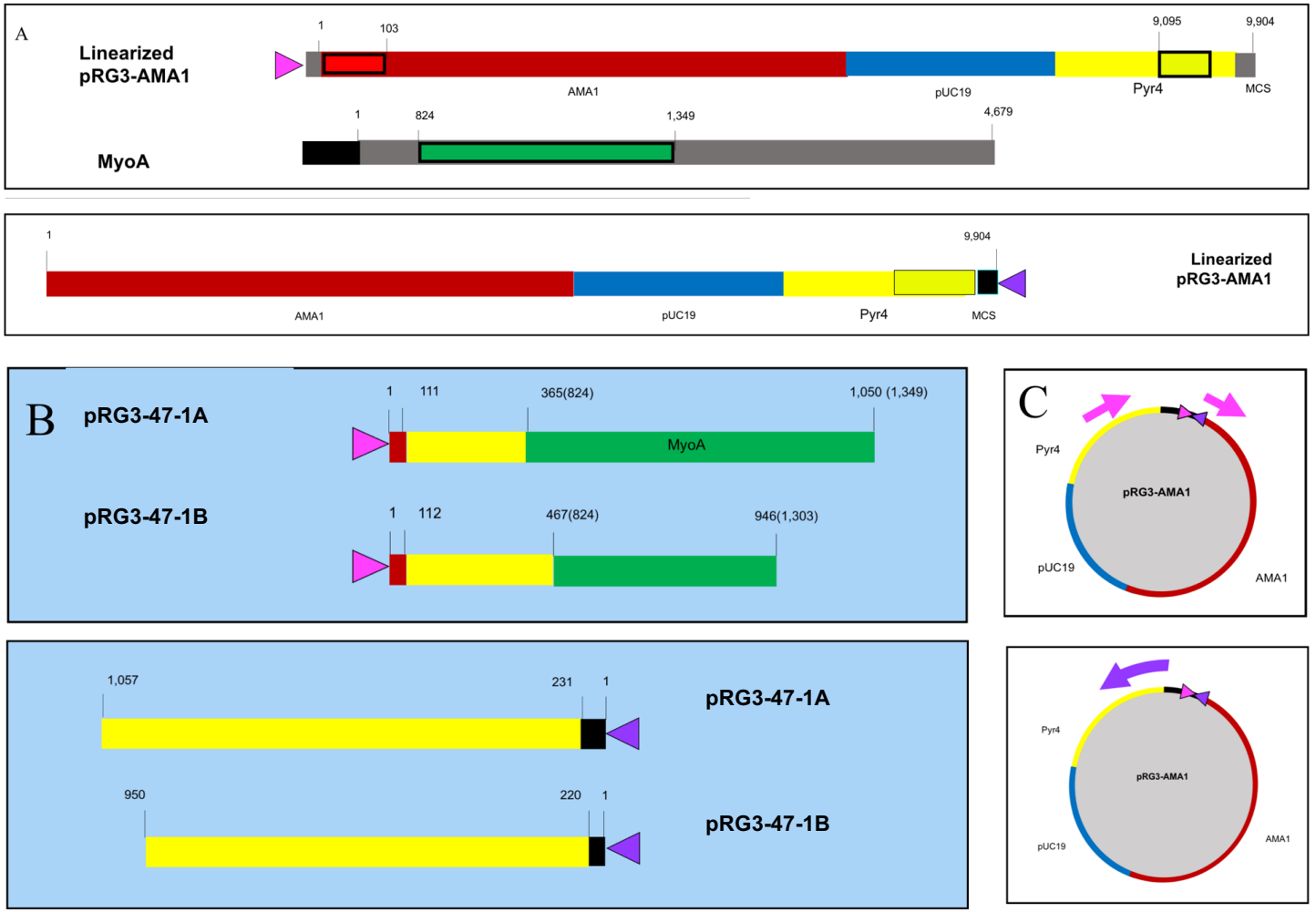

Figure 6. Sequencing of the pRG3-47-1 plasmid.
(A) These two panels describe what the expected sequencing read should look like for both the forward (top panel) and reverse pRG3-AMA1 sequencing reaction (bottom panel). Black rectangles highlight which regions of the sequenced plasmid correspond to this prediction. Each portion of the vector is color coded. Red=AMA1 sequence, Blue=pUC19, yellow=*pyr*4, and green=the sequenced portion of *myoA,* Black=MSC (B) These two panels summarize the sequencing reads of two individual clones. The numbers in parentheses describe what region of *myoA* the sequencing read aligns to. (C) These two panels describe an empty pRG3-AMA1 vector and show where M13 (pink triangle) and RG3 (purple triangle) sit in an uncut plasmid. The arrows in the corresponding color describe what regions of the vector the sequencing reaction returned.

Sub-clone of *myoA* restores polarized growth to *swoQ*

A sub-clone of *myoA* was created by cloning an A-tailed PCR amplicon of AN1558 into the pGEM®-T easy vector. Primers, MyoA Forward +1kb upstream and MyoA Reverse +1kb downstream, amplified 6,079 bp of AN1558 using A773 wild-type genomic DNA as template. This amplicon was ligated into the vector; the resulting plasmid was named pGEM-*myoA* (Table 2) and was co-transformed with pRG3-AMA1-NotI into the *swoQ* mutant. Transformants were then screened for restored *pyrG* prototrophy and restored polarized growth. Microscopic observations of *swoQ* mutants transformed with pGEM-*myoA* showed restored polarized growth at 42ºC (Figure 7). PCR with vector specific primers, T7 and SP6 (Table 3), was used to confirm if transformants possessed pGEM-*myoA* (Figure 8).

Conidia of each strain was harvested and diluted to a concentration of 103 spores/µl; 10 µl of this solution was placed in the center of a solid media plate and incubated at 30°C for five days. Following incubation, the diameter of colonies was measured on 2 axes, imaged (Figure 9) and the mean diameter of each strain recorded in Table 4. This examination was revealed a significant difference between the *swoQ* mutant, *swoQ* transformed with the pRG3-47-1, and *swoQ-myoA*. The mean colony diameter observed for each strain at the 30ºC and 42ºC are as follows, respectively: A773 wild-type strain was 510 mm and 440 mm in size, *swoQ* was 520mm and 220mm, *swoQ*-pRG3-47-1 was 540 mm and 385 mm, and *swoQ-myoA* was 525 mm and 450mm (Table 5). Statistical methods were used in order to determine if there was a significant difference between the mean diameter of the *swoQ* mutant (μ_q) at 42ºC and the mean diameter of the

swoQ-myoA strain (μ_m). To test this the difference, the null hypothesis (H_0), where the difference between μ_m and μ_q equals 0 ($H_0 = \mu_m - \mu_q = 0$), was compared against the alternative hypothesis H_a, where the difference between μ_m and μ_q is greater than 0 ($H_a = \mu_m - \mu_q \leq 0$). A two tailed t-test returned a *p*-value of .0031, based on the means of the *swoQ* mutant and the *swoQ-myoA* strain. By conventional criteria and a level of significance of .05 the difference is consistent with the null hypothesis and therefore found to be statistically significant indicating that addition of a wild-type copy of *myoA* in *swoQ* has the ability to restore polarized growth to the mutant strain.

Following assessment of the colony phenotype, conidia were collected with 2 mL of sterile water and quantified using a hemocytometer. A similar statistical approach as described in the preceding paragraph was used to assess conidia production. Conidia production was assessed between the *swoQ* mutant, wild-type, *swoQ-myoA* and A773-*myoA* strains (Table 5). This examination revealed the mean of conidia produced by the *swoQ* strain was 64.25×10^6 at 30ºC but only 9.20×10^2 at 42ºC. A two tailed t-test revealed a *p*-value of less than .0001, which by conventional criteria α=.05 this difference is statistically significant. A statistically significant difference was found between the conidia production of the *swoQ* mutant and the conidia production of the *swoQ-myoA* strain. The *p*-value for this paired t-test was found to be .0371 which by conventional criteria and a level of significance where α =.05, this difference is considered to be statistically significant. Conidia were collected from each strain as described above, and quantified (Table 9).

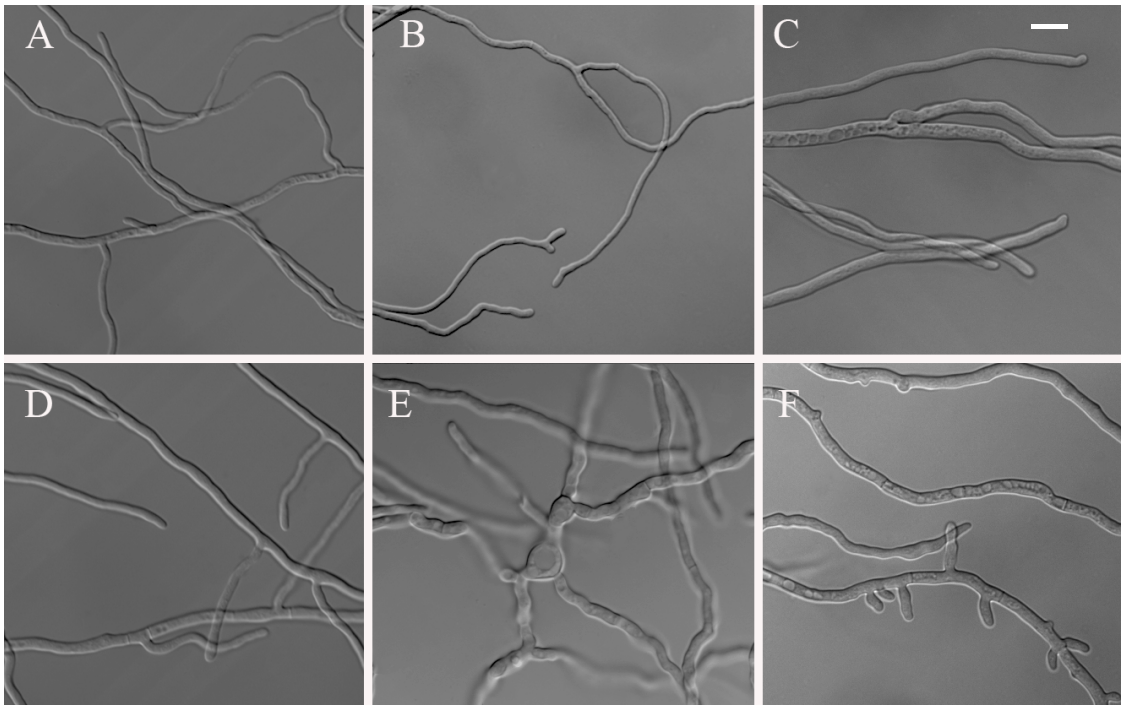

Figure 7. A sub-clone of *myoA* restores polarization to *swoQ* mutant.
To evaluate differential growth between the permissive (A-C) and the restrictive (D-E) temperatures, strains were grown at their respective temperature for 16 hours then imaged with DIC on agar blocks. (A, D) WT, (B, E) *swoQ* mutant, (C, F) *swoQ* strain transformed with pGEM-*myoA*. Scale bar=10 μm.

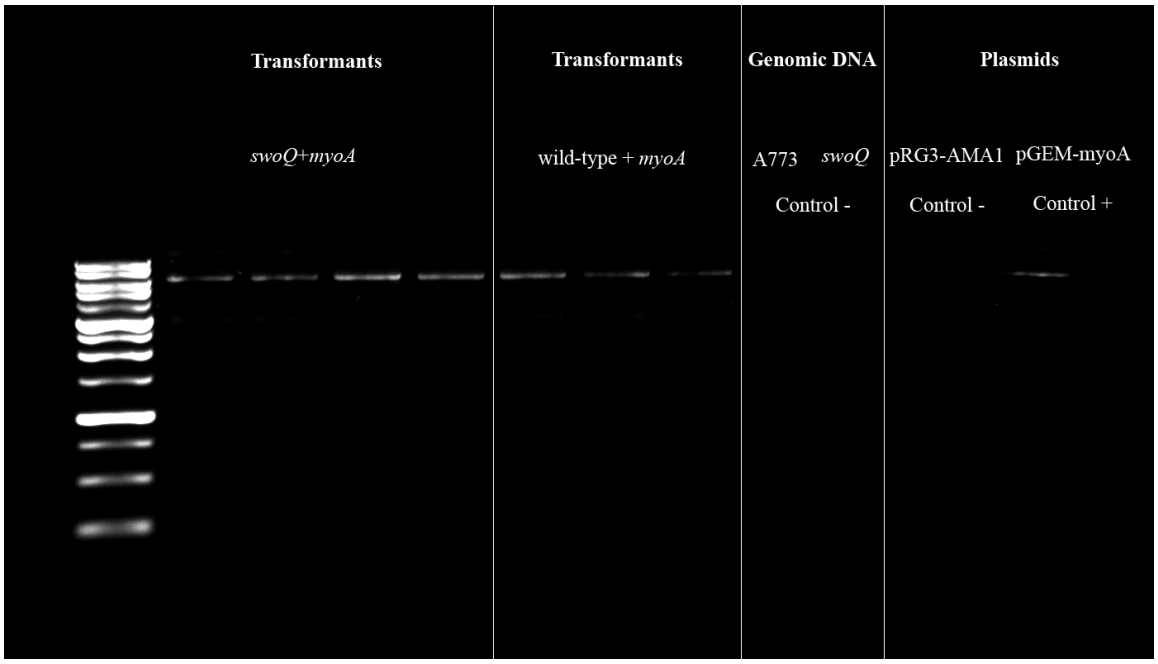

Figure 8. PCR confirmation of *myoA* transformants.
Strains transformed with pGEM-*myoA* plasmid were confirmed via PCR analysis using vector specific primers, T7 and SP6. (A) A PCR of *swoQ* strain co-transformed with pRG3-AMA1 and pGEM-*myoA* produces a 6kb fragment equivalent to the insert found in pGEM-*myoA* (B) A773 strain co-transformed with pRG3-AMA1 and pGEM-*myoA* verified via PCR analysis possesses. These strains produce a 6kb amplicon, equivalent in size to the insert the found in pGEM-*myoA* (C) Genomic DNA belonging to parent strains A773 and *swoQ* serve as a negative control and nothing is amplified. (D) A 6kb fragment is produced in a PCR using T7 and SP6 when the pGEM-*myoA* is the template and nothing is amplified from the pRG3-AMA1 plasmid.

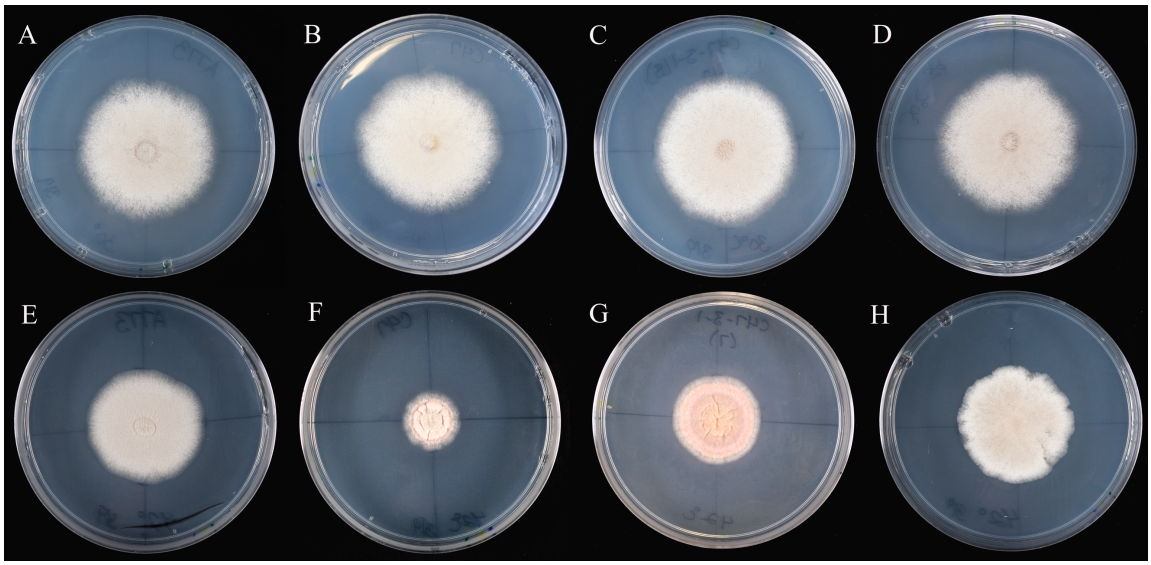

Figure 9. Colony diameter comparison between strains.
The growth diameter of the *swoQ* mutant was compared to wild-type alongside strains possessing an extra copy of *myoA*. Strains were grown for 5 days on solid media and the diameter was measured on two axes. (A-D) Strains grown at the permissive temperature. (E-H) Strains grown at the restrictive temperature. (A, E) Wild-type A773, (B, F) *swoQ* mutant (C, G) *swoQ* mutant with the pRG3-47-1 plasmid (D, H) *swoQ* strain with extra copy of wild-type *myoA*.

Table 4. Mean colony diameter following 5 days of growth.

Strain	**Relevant genotype**	**Mean diameter at 30°C**		**Mean diameter at 42°C**	
A773	WT *swoQ*	510 mm	SE=10.929	440 mm	SE=2.101
TsC-47	*swoQ* mutant	520 mm	SE=5.773	220 mm	SE=4.703
swoQ-myoA	*swoQ* + pRG3-47-1	540 mm	SE=11.112	385 mm	SE=9.962
swoQ-myoA	*swoQ* + extra copy of *myoA*	525 mm	SE=9.981	450 mm	SE=8.205

SE= Standard Error of the mean

* performed in triplicate

Table 5. Conidia production following 5 days of growth.

Strain	**Relevant genotype**	**30°C Conidia production [a]**		**42°C Conidia production**	
A773	WT *swoQ*	69.50 x 10^6	SE= 4.536	46.50 x 10^6	SE= 2.434
TsC-47	*swoQ* mutant	64.25 x 10^6	SE= 3.365	9.20 x 10^2	SE= 1.536
swoQ-MyoA	*swoQ* + extra copy of *myoA*	59. 00 x 10^6	SE=3.176	24.75 x 10^6	SE= 6.536
A773-MyoA	WT *swoQ* + extra copy of *myoA*	56.25 x 10^6	SE=2.214	33.25 x 10^6	SE=3.441

[a] Conidia production = $\bar{x}$ spores/ml ±SE

SE= Standard Error of the mean

* performed in triplicate

myoA is not defective in the *swoQ* mutant

A second round of PCR cloning and sequencing was conducted to determine if the mutation carried by *swoQ* is contained in AN1558. The *myoA* gene found in *swoQ* mutant was amplified using primers, MyoA +1kb up and MyoA +1kb down (Table 3). This PCR amplicon was then cloned into the pGEM-T easy vector system. The resulting plasmid was named pGEM-*swoQ-myoA* (Table 2). The insert was sequenced using 14 *myoA* specific primers (Table 3). Analysis of the sequence data revealed that the *myoA* allele amplified from the tsC-47 strain contains no mutant lesions and it is likely that the *swoQ* mutant lesion is elsewhere in the genome.

Overexpression of *myoA* leads to hyper-branching phenotype

The plasmid, pGEM-*myoA*, contains a sub-clone of wild-type *myoA*. This plasmid was used to overexpress AN1558 in wild-type and to determine if AN1558 is responsible for the polarization phenotype seen in the *swoQ-myoA* mutant. pGEM-*myoA* was co-transformed with pRG3-AMA1-NotI into wild-type strain, A773, in order to observe the resulting phenotype outside of the *swoQ* mutant. Transformants were then screened for restored *pyrG* prototrophy and observed microscopically for a polarization phenotype (Figure 10). Observations of the A773+extra copy *myoA* strain recovered from this transformation exhibited a hyper-branching phenotype at both 30ºC and 42ºC (Figure 10). Conidia production of the A773+extra copy *myoA* was assessed in order to determine if there was a fitness cost for carrying the pGEM-*myoA* and pRG3-AMA1-NotI plasmids (Table 5). Genomic DNA belonging to this strain was isolated and PCR verification served

to determine that the strain indeed possessed the pGEM-*myoA* plasmid (Figure 8). Hyper-branching in the A773+extra copy *myoA* strain was quantified alongside *swoQ-myoA,* A773, and *swoQ* (Table 10). A two-tailed *t*-test was performed in order to evaluate the difference of means between strains (Table 6). When compared to wild-type, mutants carrying an extra copy of *myoA* were found to vary significantly above the mean and possessed a *p*-value <.0001 at both 42ºC and 30ºC.

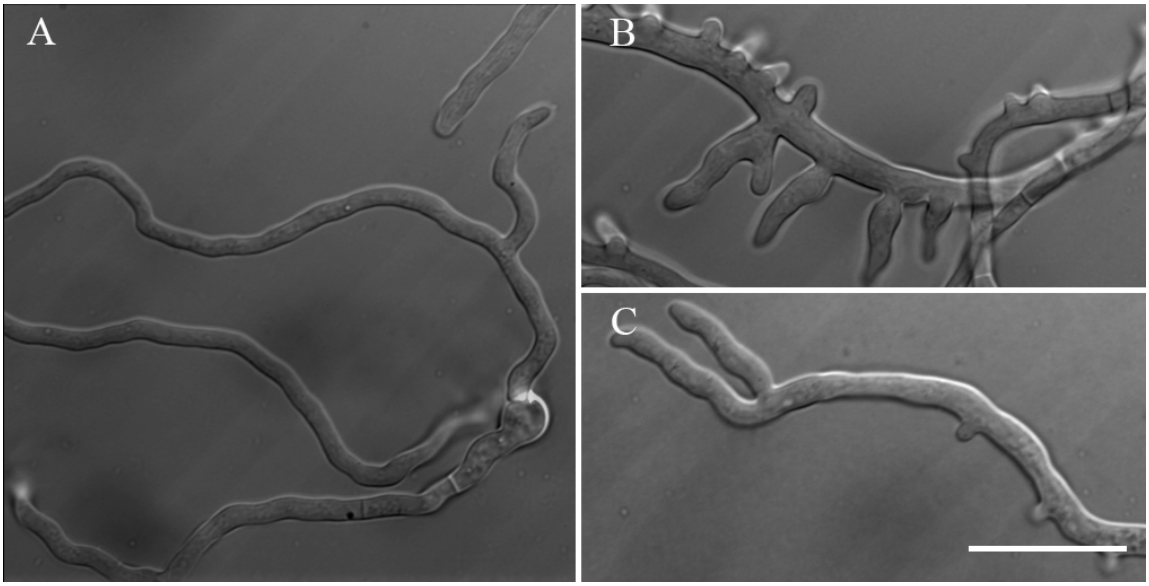

Figure 10. The overexpression of *myoA* results in hyper-branching.
Strains were grown at the restrictive temperature for 16 hours then imaged with DIC on agar blocks. (A) Wild-type A773 (B) *swoQ* mutant containing pGEM-*myoA* hyper-branches at 42ºC (B, C) A773 strain transformed with pGEM-*myoA* hyper-branches at 42ºC. Scale bar=10 µm

Table 6. Comparison of the number of branches in the first 100 microns of tip.

	Permissive temperature					Restrictive Temperature				
	A773	**swoQ**	**A773 + *myoA***	**swoQ + *myoA***	**A773 + pRG3-AMA1**	**A773**	**swoQ**	**A773 +*myoA***	**swoQ +*myoA***	**A773 + pRG3-AMA1**
Mean	0.93	0.87	1.83	4.05	0.38	1.2	0.74	3.57	5	0.67
SD*	1.01	0.99	2.04	2.97	0.59	1.33	1.04	3.08	3.01	0.86
SEMα	0.09	0.1	0.38	0.46	0.1	0.09	0.09	0.29	0.47	0.12
N	122	91	29	41	37	235	143	116	41	52
p-val.	-	.0556	.0343	<.0001	.0509	-	.975	<.0001	<.0001	.6841

SD*=Standard deviation

SEMα=Standard error of the mean

N=Sample size

p-val=two tailed t-test in comparison to wildtype A773

α=.05=less than .05 is considered statically significant

The *swoQ* locus is not genetically linked to *wetA*

The meiotic progeny of a sexual cross between the swoQ mutant strain and the *wetA* strain was analyzed to assess recombination of various markers between these two strains (Table 7). The markers followed in this experiment are *wA, argB, pyroA4, wetA,* and are found on chromosomes II, III, IV and VII, respectively. The progeny from this cross (n=51) were genotyped for each nutritional marker (*argB, pyroA4*) by replica plating on to various plates each devoid of a different nutritional marker and assessing strains for prototrophy. The *swoQ* genotype was examined by screening for the TS polarity phenotype. This involved replica plating the progeny on to two solid plates of MM plates containing all supplements and then incubating strains at either 30ºC or 42ºC. The aconidial phenotype of the *wetA* marker was assessed by plating strains at 30ºC on solid CM plates and screening for the *"wet"* phenotype associated with this allele.

The phenotype of each of the offspring was recorded and the segregation ratio between recombinants and parental alleles were assessed (Table 7). The segregation ratio of recombinants to parental alleles was used to determine if *swoQ* was found within 50 map units on chromosomes II, III, IV and VII. If one of the assessed markers is found on the same chromosome as *swoQ* then the segregation ratio would deviate significantly from 1:1. The segregation ratios observed between the *swoQ* and the *wA* allele was 21:22, *swoQ* and the *argB* allele was 24:27, *swoQ* and the *pyroA4* allele was 30:21, *swoQ* and the *wetA* allele was 25:26. Based on these data suggests the *swoQ* allele was found not to be linked to the 4 markers assessed in this study.

Table 7. Meiotic segregation of markers in the *swoQ* x *wetA* cross.

		***wA*^{II*}**		***argB*^{III*}**		***pyroA4*^{IV*}**		***wetA*^{VII*}**	
		+	-	+	-	+	-	+	-
***swoQ*^{VII}**	+	11	15	20	16	17	19	18	18
***swoQ*^{VII}**	-	6	11	11	4	11	4	8	11
Segregation Ratio[+]		21:22		24:27		30:21		25:26	
% Recombination		41%		47%		58%		49%	

*****Chromosome each marker is found

[+] Segregation Ratio=non-parental to parental progeny

Localization of polarity markers *in vivo*

The localization of various polarity markers was examined in this study. These makers included: FimA::GFP, Exo84::GFP, DnfA and DnfB. These markers were added to the *swoQ* strain in a sexual cross with the GFP strain of interest. Examination of *swoQ* FimA::GFP, at the permissive temperature has a localization similar to wild-type where FimA::GFP is enriched in the subapical collar of growing hyphae and in septa of *A. nidulans*, while at the restrictive temperature in *swoQ*, FimA::GFP displays diffuse localization throughout the hypha in comparison to wild-type (Figure 11). At the permissive temperature and in wild-type, Exo84::GFP localizes to the apical dome of growing hyphae. In contrast, at the restrictive temperature in the *swoQ* mutant, Exo84::GFP mislocalizes and appears as an amorphous matrix throughout the cytoplasm (Figure 12). In wild-type DnfA localizes to the apical PM in growing cells. In the *swoQ* mutant, DnfA was found to also localize to the apical PM but the signal is more diffuse in hyphal tips in comparison to wild-type (Figure 13). In this study DnfB was observed in the *swoQ* mutant and was found to localize to the cortex of swelling cells, while in wild-type the DnfB::GFP signal was observed to localize at a compact loci just behind the cell tip at the center of the DnfA apical structure (Figure 14).

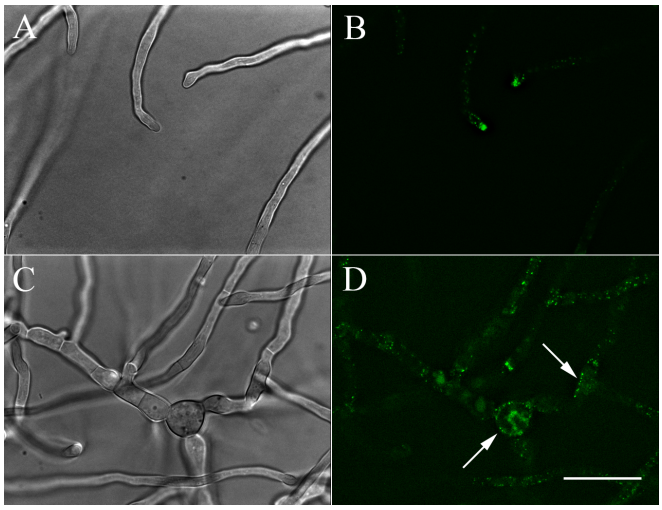

Figure 11. FimA localization is diffuse throughout hyphae in the *swoQ* mutant.
(A) *swoQ* FimA::GFP grows like wild-type at the permissive temperature. Bright-field. (B) *swoQ* FimA::GFP localizes to the subapical collar in growing cells at the permissive temperature. (C) The *swoQ*-FimA::GFP strain has swollen misshaped cells when grown at the restrictive temperature for 16 hours. (D) *swoQ*-FimA::GFP localization is diffuse throughout hyphae in the *swoQ* mutant at the restrictive temperature. Scale bar=10 µm.

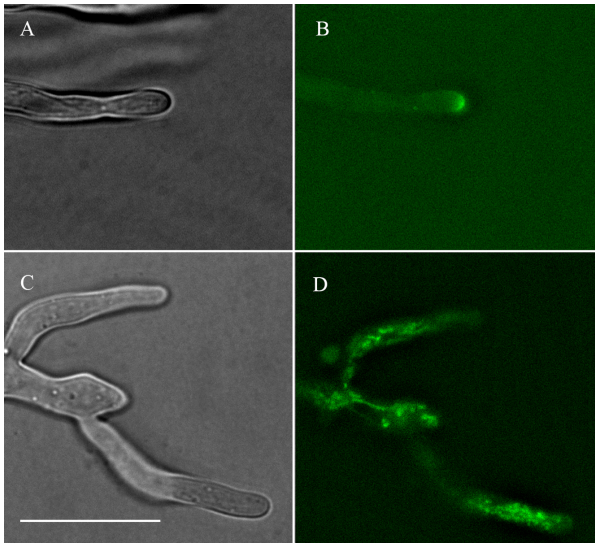

Figure 12. Exo84::GFP mislocalizes in the *swoQ* mutant.
(A) Exo84::GFP was grown at the permissive temperature (B) *swoQ* Exo84::GFP localized to the apical dome at the permissive temperature. (C) *swoQ* Exo84::GFP has swollen misshapen when was grown at the restrictive temperature. (D) At the restrictive temperature the Exo84::GFP in the *swoQ* mutant mislocalizes and appears as an amorphous matrix throughout the cytoplasm. Scale bar =10 µm.

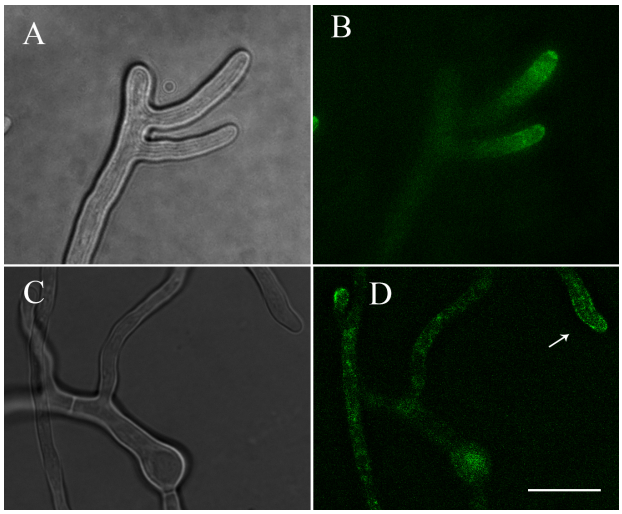

Figure 13. *swoQ* DnfA::GFP localization is more dispersed than in wild-type.
(A) DnfA::GFP grows like wild-type at the permissive temperature.(B) *swoQ* DnfA::GFP localizes to the apical PM at the permissive temperature. (C) *swoQ* DnfA::GFP has swollen misshapen cells at 42ºC following a 16 hour incubation. (D) *swoQ*::GFP localizes to the apex of the cell and has a diminished signal in comparison to wild-type. Scale bar=10 µm.

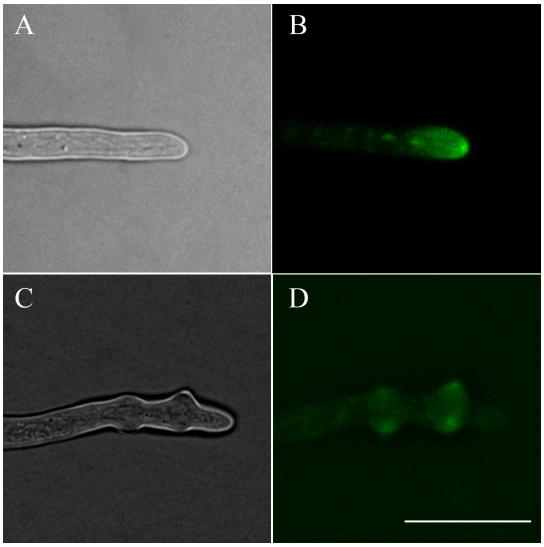

Figure 14. DnfB localizes to swollen cells in *swoQ* mutant.
(A) *swoQ* DnfB::GFP grows like wild-type at the permissive temperature. Bright-field. (B) *swoQ* DnfB::GFP localizes at a compact loci just behind the cell tip at the permissive temperature (C) *swoQ* DnfB::GFP strain has swollen misshaped cells when grown at the restrictive temperature for 16 hours. (D) DnfB::GFP localizes to the cortex of swelling cells. Scale bar=10 µm.

CHAPTER IV

CONCLUSIONS

Organization of the cytoskeleton is necessary in order to facilitate polarized hyphal growth. The cytoskeleton plays a pivotal role in the transport of secretory and endocytic vesicles in the apex of the cell. These processes are governed by MTs and F-actin and their corresponding motor proteins: kinesin, dynein, and myosin. Class I myosins, are involved in cytoskeleton-membrane interactions and we speculate they play a role in both exocytosis and endocytosis. Previous studies have established that MyoA is an important player in polarized growth and is essential in *A. nidulans (60).* In this study I examined the role of MyoA and affirmed its importance in hyphal growth by demonstrating it has a polarization affect on hyphae and that overexpression of this protein has the ability to suppress the *swoQ* polarity defect.

The work described here was designed to identify genes involved in polar growth. The tsC-47 strain, *swoQ,* was selected from a previously generated collection of *A. nidulans* TS mutants for further study because of its swollen cell polarity defect. Temperature-shift experiments showed that polar growth in the *swoQ* mutant is lost following an upshift from the permissive to the restrictive temperature, and is able to recover polar growth following a downshift from the restrictive to the permissive temperature. A genetic cross between *swoQ* and wild-type revealed that the mutant allele found in *swoQ* occurs at a single locus and segregates 1:1. The *swoQ* strain was transformed with the pRG3-AMA1 genomic library in order to identify a plasmid which contained a genomic insert capable of restoring polarized growth to *swoQ.* The plasmid

identified, pRG3-47-1, restored polarized growth to the *swoQ* strain. The genomic insert of this plasmid was sequenced and found to encode MyoA. Following this result, the *myoA* gene in the *swoQ* mutant was sequenced in order to determine if the mutant lesion was contained in this gene. No lesions were found in the *myoA* gene in *swoQ,* suggesting that the mutant defect is likely found elsewhere in the mutant genome. A sub-clone of *myoA* was transformed into *swoQ* and was found to restore polarized growth and induce branching in the *swoQ* mutant. Similarly, a sub-clone of *myoA* was transformed into the wild-type strain and was also found to induce hyper-branching. Interestingly, the polarity defect in *swoQ* was rescued when transformed with an extra copy of *myoA,* even though this gene carried no lesion in *swoQ*. Taken together these data suggest that *myoA* has a polarization affect on cells allowing MyoA to suppress the mutant allele in *swoQ*. This effect is epistatic and could be explained in a variety of ways. For example, the masking effect of *myoA* on *swoQ* could be explained if the defect is found in an unrelated gene, this gene could encode an exocyst component where a defect in an exocyst gene could induce hyper-secretion, and overexpression of MyoA causes the strain to hyper-branch which could compensate for the defect. This phenomenon could also be explained if the *swoQ* mutant is defective in a closely related gene, like another myosin or other cytoskeletal element, allowing the overexpression of *myoA* in *swoQ* to overcome the defect.

Previous examinations of MyoA determined that the protein localizes to the sub-apical collar of hyphae. At the collar, MyoA is presumed to work alongside FimA to in order to nucleate actin and form actin patches. Together these proteins provide the driving force for invagination of the membrane and facilitate endocytosis. The polarity phenotype

observed in the *swoQ* strain is consistent with previous investigations of endocytic proteins. The MyoA ortholog, Myo-1, has been shown to be an endocytic protein in *N. crassa.* The *Δmyo*-1 mutant in *N. crassa* shares a similar phenotype to *swoQ,* where both strains display a meandering appearance and a loss of polarization. I hypothesize *swoQ* to also be involved in this process, as evidenced by Figure 2, where FM4-64 internalization was altered in the *swoQ* mutant relative to wild-type.

In order to test this hypothesis and gain insight on how *swoQ* interacts with other proteins in the current *A. nidulans* growth model the *swoQ* mutant strain was crossed with a variety of polarity markers. The polarity markers assessed in this study were FimA, an actin cross-linking protein, Exo84, a component of the exocyst complex, and the flippases DnfA and DnfB which localize to secretory vesicles and play a role in asymmetrical distribution of the phospholipid phosphatidylserine at the tip. This examination revealed that *swoQ* has an affect on the localization of FimA::GFP and a major effect on the localization of Exo84::GFP *in vivo* (Figure 11 and Figure 12). In order to interpret data obtained from these experiments, these observations were integrated into the *A. nidulans* growth model (Figure 15).

Previous studies have determined the role various myosins have on fungal growth, however, an all-encompassing model describing how the cytoskeleton and myosin motor proteins cooperate with endocytic and exocytic machinery to facilitate apical recycling, has yet to be described. Due the lack of this model, I built one for this study in order to understand how MyoA overexpression restores polarized growth to *swoQ* (Figure 15). This model summarizes the various functions of the five myosins currently described in

A. nidulans. These five myosins belong to four classes (I, II, V, XVII) and each plays a different role in growth. Class I myosins, like MyoA, are responsible for exocytosis and endocytosis. MyoA has been shown to localize to sites of endocytosis where it interacts with the actin network to facilitate the formation of actin patches. Localization studies show MyoA is found at the sub-apical collar, a region of the cell associated with actin patch formation and endocytosis (*60*). Fimbrin and actin, share a similar localization pattern and likely work with MyoA to cross-link actin filaments in order to invaginate the membrane (Figure 15) (*15*). Class V myosins, like MyoE, are required for trafficking vesicles in an actin-dependent manner (*52*). In *A. nidulans,* MyoE localizes to moving puncta in the cytoplasm and SPK. This protein is likely involved in moving vesicles to the SPK. In yeast, class V myosins have been shown to be involved the transport of mRNA transcripts, mRNPs, some exocyst components, and post–Golgi vesicles (*87*). Yet these roles are not known in *A. nidulans.* The class II myosin, MyoB, has been shown to localize to septa to form septal rings and is implicated in cytokinesis and septum formation (*52*). *A. nidulans* possesses two class XVII myosins, CsmA and CsmB. This class of myosins is specific to fungi and possesses both a myosin motor domain and a chitin synthase domain (*88*). Data suggests that these myosins play a role in exocytosis by transporting chitin synthase-attached vesicles to the growth region (*88, 89*). The localization of CsmA and CsmB at hyphal tips, is dependent on an actin-binding motor domain which is implicated in the delivery of secretory vesicles at the tip. The exact mechanism which CsmA and CsmB utilizes to coordinate the delivery of secretory vesicles is unclear.

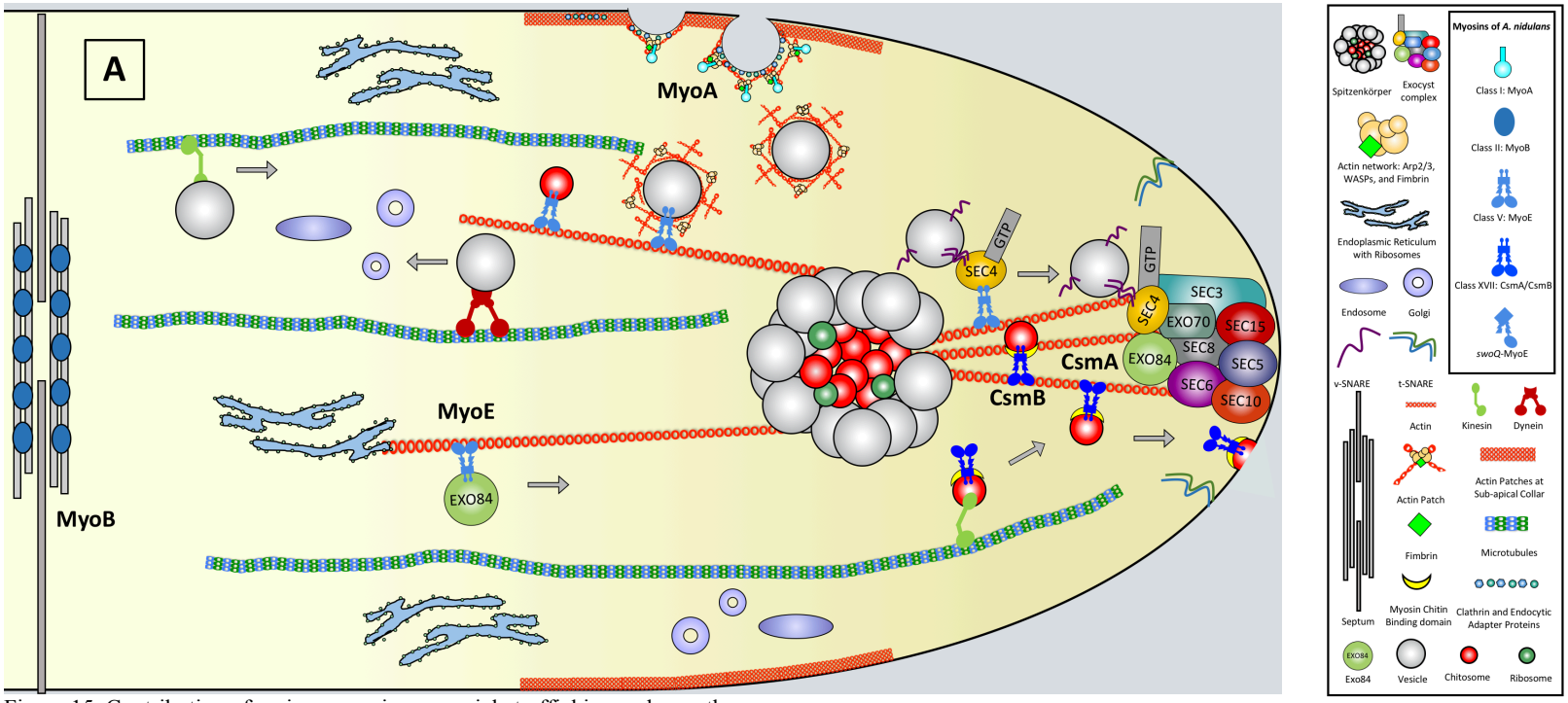

Figure 15. Contribution of various myosins on vesicle trafficking and growth.
(A) An overview of a hypothetical hyphal apex displays the cytoskeleton and various motor proteins participating in polarized growth. Two different types of motor proteins interact with MTs (green and blue chains): kinesin (green motor protein) and dynein (red motor protein). Five different myosin motor proteins (various shades of blue), which bind to actin (red chains), have been identified in *A. nidulans*. These myosins maintain polarized growth by facilitating both endocytosis and exocytosis. MyoA (cyan) localizes at the subapical collar and is associated with the nucleation of actin which stimulates the formation of the actin network (tan spheres and green square) and patch formation (red web) around sites of endocytosis. Endocytic vesicles fuse with endosomes (purple oval). Molecules delivered to endosomes are either recycled back to Golgi (purple rings) or continue on to lysosomes. MyoE (light blue) localizes to moving puncta in the cytoplasm and SPK (large collection of white, red, and green spheres). This myosin is required for trafficking vesicles (white spheres) along the actin cytoskeleton and bringing secretory vesicles to the tip. The exocyst complex (collection of multicolored pill-shaped proteins) is an octameric protein complex located at the tip of the cell which tethers secretory vesicles to the PM prior to vesicle fusion. It is hypothesized that some exocyst components, like Exo84 (green sphere), are transported by MyoE along this machinery following exit from the endoplasmic reticulum (ER) (pastel blue globular cisternae with small green ribosomes). v-SNAREs (purple wavy line) found on the secretory vesicles interact with t-SNAREs (blue and green wavy line) at the PM to mediate vesicle fusion. MyoB (dark Blue) localizes to septa and is implicated in cytokinesis and septum formation. Class XVII myosins, CsmA and CsmB (cobalt blue), possesses both a myosin motor domain and a chitin synthase domain and are associated with chitin deposition and delivery of chitosomes at the apex. It is hypothesized, CsmA is transported to the tip on a hypothetical kinesin then the CsmA myosin motor domain binds to actin facilitating a switch from the MT cytoskeleton.

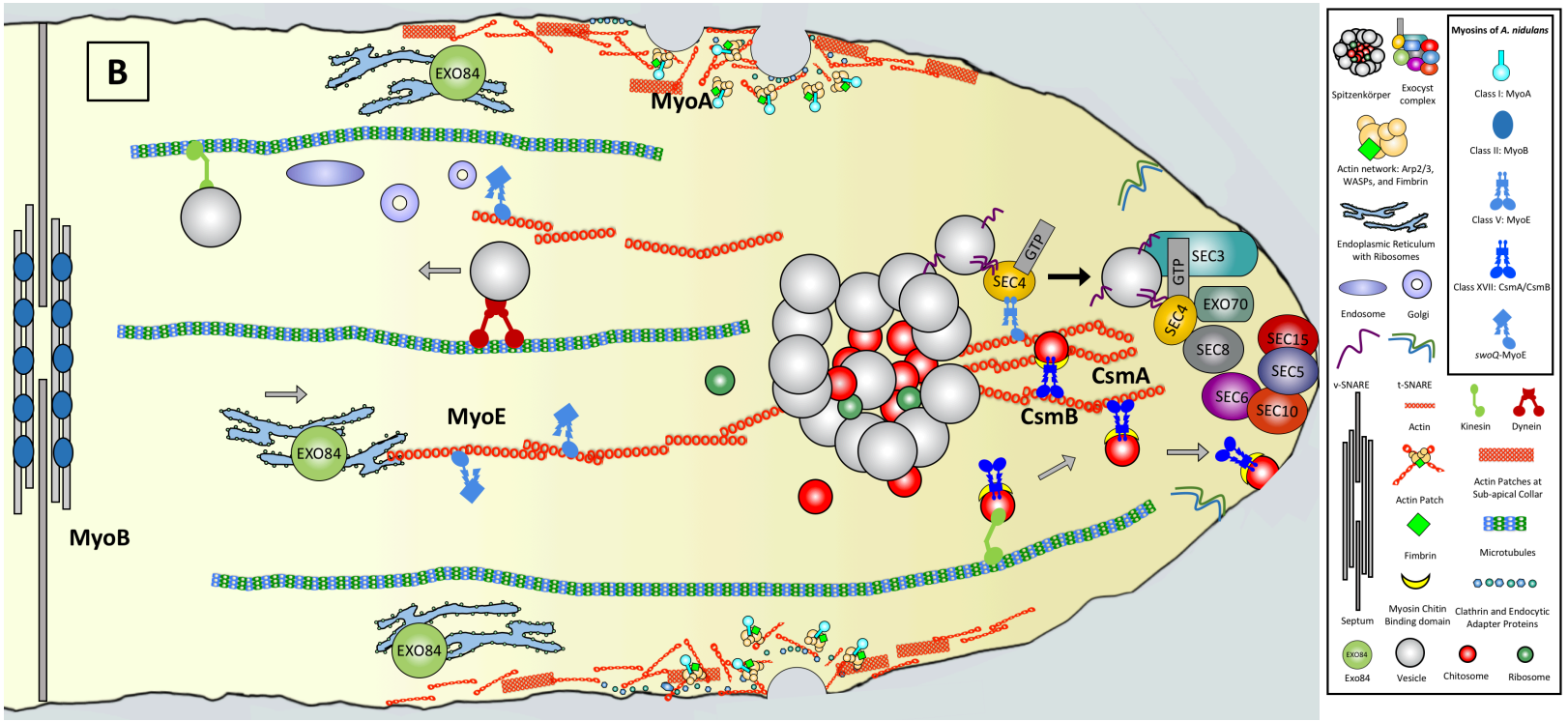

Figure 15. Continued.

(B) An overview of a hypothetical *swoQ* hyphal apex. The *swoQ* mutant displays a defect in polarized growth (misshaped hyphae) which contributes to disorganization of the actin cytoskeleton and an inability to traffic the Exo84 exocyst component (green sphere) to the tip of the cell. Due a disorganization of the actin cytoskeleton (red chains are jagged, broken and disconnected) the SPK is disordered (disorganized collection of vesicles in tip). Due to the observed localization pattern of Exo84 in the *swoQ* mutant, it is hypothesized that secretion of this protein is blocked and unable to exit the ER following synthesis by the ribosomes (green spheres overlapping pastel blue globular cisternae). It is hypothesized traffic of this protein is disrupted from the ER due to a mutant version of MyoE (*swoQ*-MyoE) (light blue and misshaped version of MyoE which is missing a motor domain and possesses an abnormal cargo binding domain). It is hypothesized that mislocalization of Exo84 in *swoQ* would lead to a disruption in the exocyst complex (disordered collection of multi-colored pill-shaped proteins at tip of cell). FimA (neon green squares) displays diffuse localization throughout the cortex in the *swoQ* mutant and is unable to assemble a well-defined sub-apical collar (scattered and diffuse actin towards cell periphery). Which is a phenotype similar to the *N. crassa Δmyo-1* mutant. Together these observations suggest that the *"swo"* phenotype is attributed to the loss of exocyst function and disorganization of the actin cytoskeleton.

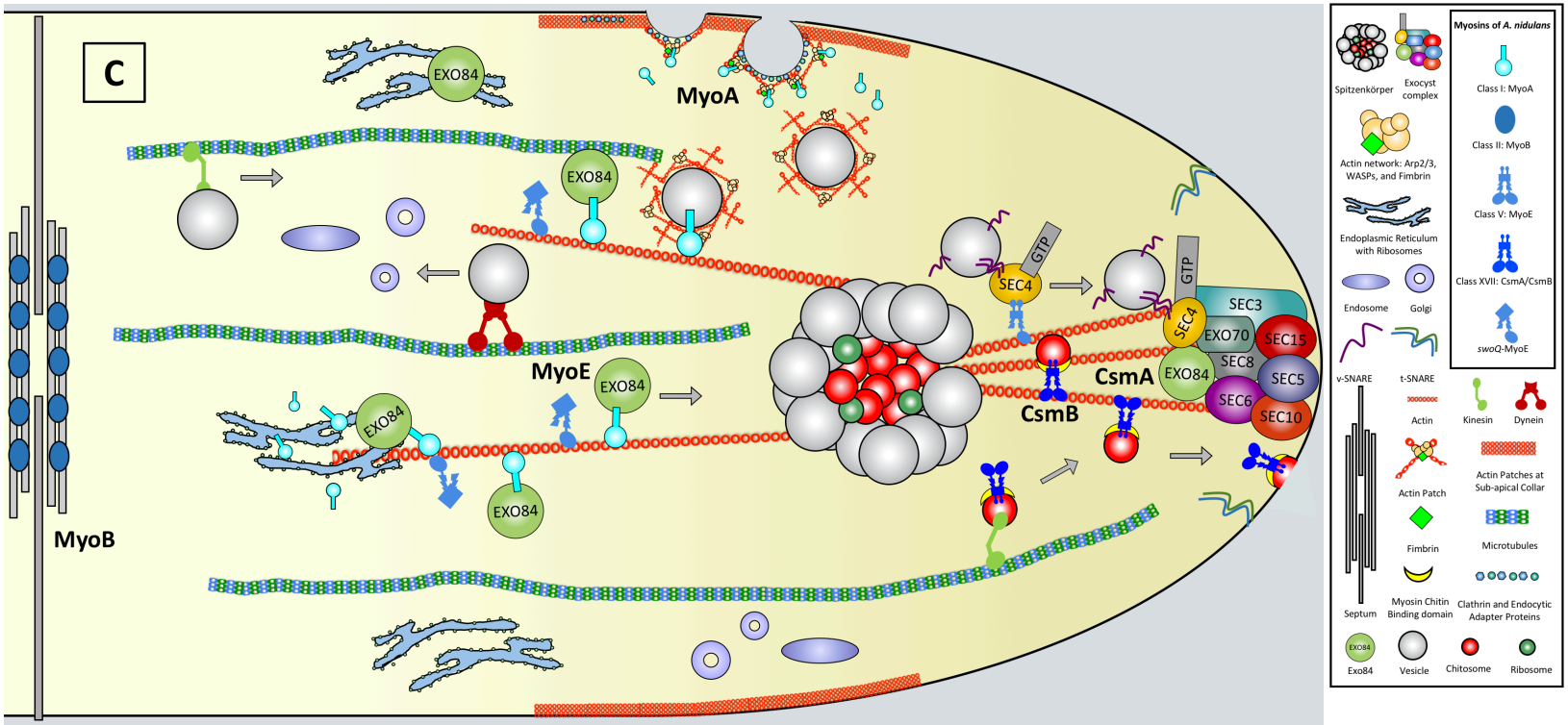

Figure 15. Continued.

(C) Overexpression of MyoA restores polarized growth to the *swoQ* mutant. An excess of MyoA in the cell (cyan myosin found throughout the cell) allows the *swoQ* to overcome its growth defect (evenly shaped hyphae) by rescuing the function of the exocyst complex and the organization of the actin cytoskeleton. Excessive expression of MyoA assists (cyan MyoA binds to vesicles and moves along actin filament) the defective protein, *swoQ*-MyoE (light blue and misshaped version of MyoE), by aiding in the transport of components needed for growth toward the tip. With the help of MyoA the secretion of Exo84 (green sphere) in the *swoQ* mutant is no longer blocked and the exocyst protein is able to exit the ER (via MyoA). Since Exo84 is able to associate with the rest of the exocyst complex the complex is no longer disrupted (organized collection of multi-colored pill-shaped proteins at the tip of the cell). Extra MyoA is hypothesized to assist in the nucleation of actin in the mutant which leads to the restoration of the actin network (tan spheres and neon green fimbrin square), the assembly of actin patches (red web) around sites of endocytosis (leading to a well-defined sub-apical collar, red blocks), and the organization of actin filaments (red chains). The presence of an organized actin cytoskeleton rescues the disrupted supply of vesicles at the tip of the cell leading to the formation of a well-organized SPK.

The delivery of CsmA at the tip is MT dependent, presumably facilitated by an unknown kinesin motor, and that the myosin motor domain acts an anchor at the tip (Figure 15) (*18, 88, 90*).

FimA and Exo84 are involved in polarized growth and when grown at 42ºC the localization of these polarity proteins are mislocalized in the *swoQ* mutant (Figure 11 and Figure 14). The localization of these proteins in both wild-type and the mutant is outlined in the Myosin growth model (Figure 15). The exocyst complex component, Exo84, localizes to the apical dome in wild-type, while in the *swoQ* mutant Exo84 appears as an amorphous matrix. This matrix is consistent with the shape of the endoplasmic reticulum (ER) in fungi (Figure 11). Due to the observed localization pattern of Exo84 and the *swoQ* phenotype, I speculate that secretion of this protein is blocked and is unable to exit the ER following synthesis by ribosomes. Exo84 remains in the ER due an uncharacterized block in exit from the ER. In addition to the mislocalization of Exo84, FimA displays diffuse localization throughout the cortex in the *swoQ* mutant and in comparison to wild-type is unable to assemble a well-defined sub-apical collar. Together these observations suggest that the *"swo"* phenotype is attributed to the loss of exocyst function and disorganization of the actin cytoskeleton. Accumulation of Exo84 in the ER suggests that *swoQ* may encode a protein associated with the trafficking of secretory vesicles from the ER to the SPK. This is consistent with previous evidence found in nerve cells where class V myosins transport vesicles from the ER in an actin dependent manner (*91, 92*). A similar protein would be necessary in *A. nidulans* in order to transport vesicles from the ER. This hypothesized protein is likely related to MyoE, a class V myosin involved in the secretion,

which possesses a deletion phenotype similar to the *swoQ* mutant *(52)*. This theory is supported by the fact that MyoA is involved in secretion and overexpression of this protein is capable of overcoming the *swoQ* polarity defect. I hypothesize that overexpression of MyoA is suppressing a mutation in another myosin, possibly MyoE. Overexpression of MyoA would increase secretion in the *swoQ* mutant which would compensate for the lack of this hypothesized myosin protein and overcome the observed exocytosis defect.

Future directions

These data suggest that the mutant allele found in *swoQ* inhibits proper exocytosis. The abnormal localization pattern of FimA and Exo84 in the *swoQ* mutant suggests the transport of secretory vesicles from the ER is blocked due to an unknown defect in *swoQ*. Identification of the gene encoded by *swoQ* is necessary to better understand the transport of secretory vesicles and exocytosis during polarized growth.

In the previous section I described how overexpression of MyoA is able to suppress the *swoQ* mutation which is likely found in another myosin, most likely MyoE. In order to test this hypothesis, I need to sub-clone and sequence a copy of the *myoE* gene found in the *swoQ* mutant. This experiment will aid in determining if *swoQ* possesses a mutant copy of *myoE*. If the *swoQ* strain is found to possess a mutant copy of *myoE*, I can proceed by seeing if a wild-type copy of this gene can complement the *swoQ* polarity defect. If a mutant lesion is not found to be encoded within *myoE* and *swoQ* is found to possess a wild-type copy of this gene, the scope of this experiment can be broadened to include *myoB, csmA,* and *csmB*. These other myosins can be sub-cloned and sequenced in

order to identify the defective gene. If this broad examination of myosins in *swoQ* does not identify the mutant allele, I can follow up this experiment by revisiting the forward genetic approach used to identify MyoA as a suppressor.

The s*woQ* gene was not identified in this forward genetic screen but instead an extragenic suppressor was identified. A library plasmid which complements *swoQ* was not identified in this initial screen due to the small sample size of screened transformants, where only 1,400 prototrophic transformants were examined in this study. This small sample size could account for an incomplete representation of the genomic library. In order to ensure full representation of the library a large number of transformants needs to be screened. The library used in this study contained 3,333 different types of plasmids and in order to ensure at least 90% of the plasmid types in the mixture are represented I would need to screen ~10,000 transformants (*93*). By recovering more transformants, I would ensure full representation of the genomic library and likely identify *swoQ*.

In the event that *swoQ* is not represented in the genomic library, another way to identify the mutant allele in *swoQ* is through mitotic mapping. Unlike meiotic mapping, where the genetic linkage of widely separated genes is difficult to establish, mitotic mapping can be used to determine on which chromosome *swoQ* resides and determine the linkage of genes which are far apart on the same chromosome (*77*). The first step in mitotically mapping involves the formation of a diploid. To make a diploid *swoQ,* a heterokaryon needs to be formed with a mapping strain with a screenable nutritional marker on each chromosome. Through an uncharacterized mechanism, diploid condia are spontaneously formed. This diploid can then be isolated. Through parasexual genetics

haploidized diploids will be screened in order to trace which genes are linked and which genes sort independently. Mitotic disjunction makes heterozygous genes distal to the crossover homozygous, therefore the frequencies of different homozygous classes can be used to determine gene order and the relative map distance between *swoQ* other markers in the experiment. Once the chromosomal location of *swoQ* is determined, this data can then be compared to a chromosome map and by looking at the region *A. nidulans* reference genome an informed decision can be made to determine which genes should be analyzed further in order to determine what gene *swoQ* encodes.

A more straightforward approach for identifying the mutant defect in *swoQ* would entail sequencing the entire genome of the mutant. Next-generation sequencing would allow for me to map the entire genome of *swoQ* in search for the mutant allele. Since many single nucleotide polymorphisms could be present in the laboratory strain, a backcross to the wild-type strain is necessary to get rid of uncharacterized mutations. Progeny from this cross, displaying the *swoQ* phenotype can then be sequenced. The sequence reads generated from whole genome sequencing would then be aligned to the *A. nidulans* reference genome. Concatenated sequence data can then be used to directly compare the *swoQ* mutant to the wild-type reference genome in order to reveal the exact polymorphism contributing to the observed polarity defect.

Once *swoQ* is identified, I would like to examine how *swoQ* plays into the current growth model. To do this I would first examine the localization of the protein encoded by *swoQ* protein using GFP, and determine examine how it associates with other proteins. The first proteins I would colocalize alongside SwoQ::GFP would be MyoA. Since *swoQ*

is thought to encode another myosin colocalization with MyoA inside of both wild-type and complemented mutant would likely reveal how MyoA overexpression is able to compensate the defect. Results from this experiment could provide a better understanding of the role of MyoA in secretion and how SwoQ cooperates with other myosins to facilitate polarized growth. In *A. nidulans* it is currently poorly understood how proteins are trafficked from the ER, and what cytoskeletal elements these secretory proteins utilize during transit proteins. Based on the data examined in this study, SwoQ plays a role in the secretion of Exo84 from the ER. The mechanism behind secretion from the ER can be elucidated in future studies of SwoQ. By tracing the localization of SwoQ::GFP at the ER and then colocalizing this protein alongside ActA::GFP a connection between actin and SwoQ can be formed. I hypothesize SwoQ can be visualized carrying cargo along actin filaments from the ER. The localization of Exo84 from the ER can be compared to SwoQ::GFP in order to determine if this exocyst component is cargo of SwoQ.

The experiments conducted in this study revealed an interesting association between myosin motor proteins and exocytosis from the ER. Currently this process is not fully understood in *A. nidulans* and the experiments proposed in this study have the potential to decipher the mechanism involved in secretion from the ER and will better the understanding of how polarized growth is maintained in *A. nidulans.*

REFERENCES

1. D. G. Drubin, W. J. Nelson, Origins of cell polarity. *Cell* **84**, 335-344 (1996).
2. S. Bartnicki-Garcia, Cell wall chemistry, morphogenesis, and taxonomy of fungi. *Annual Review of Microbiology* **22**, 87-108 (1968).
3. H. Brunswick. Untersuchungen über die geschlechts-und kernverhältnisse bei der *Hymenomyzeten* gattung *Coprinus*: mit 35 Tabellen. *Goebel* **5**. 1-152 (1924).
4. M. Bastmeyer, H. B. Deising, C. Bechinger, Force exertion in fungal infection. *Annual Review of Biophysics and Biomolecular Structure* **31**, 321-341 (2002).
5. J. E. Galagan, S.E. Calvo, C. Cuomo, L.J. Ma, J.R. Wortman, Sequencing of *Aspergillus nidulans* and comparative analysis with *A. fumigatus* and *A. oryzae*. *Nature* **438**, 1105-1115 (2005).
6. S. Bartnicki-Garcia, D. D. Bartnicki, G. Gierz, R. López-Franco, C. E. Bracker, Evidence that Spitzenkörper behavior determines the shape of a fungal hypha: a test of the hyphoid model. *Experimental Mycology* **19**, 153-159 (1995).
7. S. Bartnicki-Garcia, C. E. Bracker, G. Gierz, R. López-Franco, H. Lu, Mapping the growth of fungal hyphae: orthogonal cell wall expansion during tip growth and the role of turgor. *Biophysical Journal* **79**, 2382-2390 (2000).
8. S. N. Grove, C. E. Bracker, D. J. Morre, An ultrastructural basis for hyphal tip growth in *Pythium ultimum*. *American Journal of Botany*, 245-266 (1970).
9. R. J. Howard, Ultrastructural analysis of hyphal tip cell growth in fungi: Spitzenkörper, cytoskeleton and endomembranes after freeze-substitution. *Journal of Cell Science* **48**, 89-103 (1981).

10. S. Bartnicki-Garcia, D. D. Bartnicki, G. Gierz, Determinants of fungal cell wall morphology: the vesicle supply center. *Canadian Journal of Botany* **73**, 372-378 (1995).

11. J. Verdin, S. Bartnicki-Garcia, Functional stratification of the Spitzenkörper of *Neurospora crassa*. *Molecular Microbiology* **74**, 1044-1053 (2009).

12. S. Bartnicki-Garcia, Hyphal tip growth: outstanding questions. *Mycology Series* **15**, 29-58 (2002).

13. J. H. Sietsma, J. G. H. Wessels, Growth, differentiation and sexuality: apical wall biogenesis. in *The Mycota* **1**, J. G. H. Wessels, F. Meinhardt, Eds., Springer Berlin Heidelberg, 125-141 (1994).

14. A. Pantazopoulou, M. Pinar, X. Xiang, M. A. Penalva, Maturation of late Golgi cisternae into RabE(RAB11) exocytic post-Golgi carriers visualized *in vivo*. *Molecular Biology of the Cell* **25**, 2428-2443 (2014).

15. Z. Schultzhaus, L. Quintanilla, A. Hilton, B. D. Shaw, Live-cell imaging of actin dynamics in the filamentous fungus *Aspergillus nidulans*. *Microscopy and Microanalysis* **22**, 264-274 (2016).

16. S. D. Harris, L. Hamer, K. E. Sharpless, J. E. Hamer, The *Aspergillus nidulans sepA* gene encodes an FH1/2 protein involved in cytokinesis and the maintenance of cellular polarity. *The European Molecular Biology Organization Journal* **16**, 3474-3483 (1997).

17. A. Virag, S. D. Harris, The Spitzenkörper: a molecular perspective. *Mycological Research* **110**, 4-13 (2006).

18. G. Steinberg, Hyphal growth: a tale of motors, lipids, and the Spitzenkörper. *Eukaryotic Cell* **6**, 351-360 (2007).

19. E. Sánchez-León, J. Verdín, M. Freitag, R.W. Roberson, S. Bartnicki-Garcia, M. Riquelme, Traffic of chitin synthase 1 (CHS-1) to the Spitzenkörper and developing septa in hyphae of *Neurospora crassa*: actin dependence and evidence of distinct microvesicle populations. *Eukaryotic Cell* **10**, 683-695 (2011).

20. Z. Schultzhaus, H. Yan, B. D. Shaw, *Aspergillus nidulans* flippase DnfA is cargo of the endocytic collar, and plays complementary roles in growth and phosphatidylserine asymmetry with another flippase, DnfB. *Molecular Microbiology* **97**, 18-32 (2015).

21. S. D. Harris, N.D. Read, R.W. Roberson, B.D. Shaw, S. Seiler, M. Plamann, M. Momany, Polarisome meets Spitzenkörper: microscopy, genetics, and genomics converge. *Eukaryotic Cell* **4**, 225-229 (2005).

22. J. E. Irazoqui, A. S. Gladfelter, D. J. Lew, Cdc42p, GTP hydrolysis, and the cell's sense of direction. *Cell Cycle* **3**, 861-864 (2004).

23. R. Fischer, N. Zekert, N. Takeshita, Polarized growth in fungi-interplay between the cytoskeleton, positional markers and membrane domains. *Molecular Microbiology* **68**, 813-826 (2008).

24. S. D. Harris, M. Momany, Polarity in filamentous fungi: moving beyond the yeast paradigm. *Fungal Genetics and Biology* **41**, 391-400 (2004).

25. K. E. Sharpless, S. D. Harris, Functional characterization of the *Aspergillus nidulans* formin SepA. *Molecular Biology of the Cell* **13**, 469-479 (2002).

26. A. C. Brand, E. Morrison, S. Milne, S. Gonia, C. A. Gale, N. A. R. Gow, Cdc42 GTPase dynamics control directional growth responses. *Proceedings of the National Academy of Sciences* **111**, 811-816 (2014).

27. H. C. Hoch, R. C. Staples, B. Whitehead, J. Comeau, E. D. Wolf, Signaling for growth orientation and cell differentiation by surface topography in *Uromyces*. *Science* **235**, 1659-1662 (1987).

28. B. He, W. Guo, The exocyst complex in polarized exocytosis. *Current opinion in Cell Biology* **21**, 537-542 (2009).

29. F. Finger, P. Novick, Spatial regulation of exocytosis: lessons from yeast. *The Journal of Cell Biology* **142**, 609-612 (1998).

30. L. M. Machesky, K. L. Gould, The Arp2/3 complex: a multifunctional actin organizer. *Current Opinion in Cell Biology* **11**, 117-121 (1999).

31. J. H. Lipschutz, K. E. Mostov, Exocytosis: the many masters of the exocyst. *Current Biology* **12**, 212-214 (2002).

32. M. Riquelme, E. L. Bredeweg, O. Callejas-Negrete, R. W. Roberson, S. Ludwig, The *Neurospora crassa* exocyst complex tethers Spitzenkörper vesicles to the apical plasma membrane during polarized growth. *Molecular Biology of the Cell* **25**, 1312-1326 (2014).

33. A. Hervas-Aguilar, M. A. Penalva, Endocytic machinery protein SlaB is dispensable for polarity establishment but necessary for polarity maintenance in hyphal tip cells of *Aspergillus nidulans*. *Eukaryotic Cell* **9**, 1504-1518 (2010).

34. B. D. Shaw, S. Upadhyay, *Aspergillus nidulans swoK* encodes an RNA binding protein that is important for cell polarity. *Fungal Genetics and Biology* **42**, 862-872 (2005).

35. D. Caballero-Lima, I. N. Kaneva, S. P. Watton, P. E. Sudbery, C. J. Craven, The spatial distribution of the exocyst and actin cortical patches is sufficient to organize hyphal tip growth. *Eukaryotic Cell* **12**, 998-1008 (2013).

36. D. R. TerBush, P. Novick, Sec6, Sec8, and Sec15 are components of a multisubunit complex which localizes to small bud tips in *Saccharomyces cerevisiae*. *The Journal of Cell Biology* **130**, 299-312 (1995).

37. R. Jahn, T. C. Sudhof, Membrane fusion and exocytosis. *Annual Review of Biochemistry* **68**, 863-911 (1999).

38. J. Schmid, F. M. Harold, Dual roles for calcium ions in apical growth of *Neurospora crassa*. *Journal of General Microbiology* **134**, 2623-2631 (1988).

39. J. Mulholland, J. Konopka, B. Singer-Kruger, M. Zerial, Visualization of receptor-mediated endocytosis in yeast. *Molecular Biology of the Cell* **10**, 799-817 (1999).

40. B. D. Shaw, D. Chung, C. Wang, L. A. Quintanilla, S. Upadhyay, A role for endocytic recycling in hyphal growth. *Fungal Biology* **115**, 541-546 (2011).

41. F. Lara-Rojas, S. Bartnicki-García, R. R. Mouriño-Pérez, Localization and role of MYO-1, an endocytic protein in hyphae of *Neurospora crassa*. *Fungal Genetics and Biology* **88**, 24-34 (2016).

42. S. Upadhyay, B. D. Shaw, The role of actin, fimbrin and endocytosis in growth of hyphae in *Aspergillus nidulans*. *Molecular Microbiology* **68**, 690-705 (2008).

43. N. Taheri-Talesh, T. Horio, L. Araujo-Bazan, X. Dou,The tip growth apparatus of *Aspergillus nidulans*. *Molecular Biology of the Cell* **19**, 1439-1449 (2008).

44. A. E. Adams, D. Botstein, D. G. Drubin, Requirement of yeast fimbrin for actin organization and morphogenesis *in vivo*. *Nature* **354**, 404-408 (1991).

45. E. Kübler, H. Riezman, Actin and fimbrin are required for the internalization step of endocytosis in yeast. *The European Molecular Biology Organization Journal* **12**, 2855-2862 (1993).

46. G. Vaduva, N. C. Martin, A. K. Hopper, Actin-binding verprolin is a polarity development protein required for the morphogenesis and function of the yeast actin cytoskeleton. *The Journal of Cell Biology* **139**, 1821-1833 (1997).

47. A. Balguerie, P. Sivadon, M. Bonneu, M. Aigle, Rvs167p, the budding yeast homolog of amphiphysin, colocalizes with actin patches. *Journal of Cell Science* **112**, 2529-2537 (1999).

48. D. Pruyne, A. Bretscher, Polarization of cell growth in yeast. I. Establishment and maintenance of polarity states. *Journal of Cell Science* **113**, 365-375 (2000).

49. J. B. Moseley, B. L. Goode, The yeast actin cytoskeleton: from cellular function to biochemical mechanism. *Microbiology and Molecular Biology Reviews* **70**, 605-645 (2006).

50. J. Zhang, S. Li, R. Fischer, X. Xiang, Accumulation of cytoplasmic dynein and dynactin at microtubule plus ends in *Aspergillus nidulans* is kinesin dependent. *Molecular Biology of the Cell* **14**, 1479-1488 (2003).

51. E. B. Lewellyn, D. G. Drubin, Investigating the function of class-I myosin motors during endocytosis in Saccharomyces cerevisiae, *Molecular Biology of the Cell* **23**, 1059-1524 (2012).

52. N. Taheri-Talesh, Y. Xiong, B. R. Oakley, The functions of myosin II and myosin V homologs in tip growth and septation in *Aspergillus nidulans*. *PLoS One* **7**, 312-318 (2012).

53. H. Renshaw, J. M. Vargas-Muniz, A. D. Richards, Y. G. Asfaw, P. R. Juvvadi, Distinct roles of myosins in *Aspergillus fumigatus* hyphal growth and pathogenesis. *Infectious Immunity* **84**, 1556-1564 (2016).

54. N. Osherov, G. May, Conidial germination in *Aspergillus nidulans* requires RAS signaling and protein synthesis. *Genetics* **155**, 647-656 (2000).

55. F. Z. Idrissi, H. Grötsch, I. M. Fernández-Golbano, C. Presciatto-Baschong, H. Riezman, Distinct acto/myosin-I structures associate with endocytic profiles at the plasma membrane. *The Journal of Cell Biology* **180**, 1219-1232 (2008).

56. Y. Sun, A. C. Martin, D. G. Drubin, Endocytic internalization in budding yeast requires coordinated actin nucleation and myosin motor activity. *Developmental Cell* **11**, 33-46 (2006).

57. B. L. Anderson, I. Boldogh, M. Evangelista, C. Boone, L. A. Greene, The Src homology domain 3 (SH3) of a yeast type I myosin, Myo5p, binds to verprolin and is required for targeting to sites of actin polarization. *The Journal of Cell Biology* **141**, 1357-1370 (1998).

58. M. G. Smith, S. R. Swamy, L. A. Pon, The life cycle of actin patches in mating yeast. *Journal of Cell Science* **114**, 1505-1513 (2001).

59. F. Z. Idrissi, A. Blasco, A. Espinal, M. I. Geli, Ultrastructural dynamics of proteins involved in endocytic budding. *Proceedings of the National Academy of Sciences of the United States of America* **109**, 2587-2594 (2012).

60. C. A. McGoldrick, C. Gruver, G. S. May, *myoA* of *Aspergillus nidulans* encodes an essential myosin I required for secretion and polarized growth. *The Journal of Cell Biology* **128**, 577-587 (1995).

61. X. Liu, N. Osherov, H. Brzeska, G. S. May, Myosin I mutants with only 1% of wild-type actin-activated MgATPase activity retain essential in vivo function(s). *Proceedings of the National Academy of Sciences* **98**, 9122-9127 (2001).

62. T. Horio, B. R. Oakley, The role of microtubules in rapid hyphal tip growth of *Aspergillus nidulans*. *Molecular Biology of the Cell* **16**, 918-926 (2005).

63. C. E. Oakley, B. R. Oakley, Identification of gamma-tubulin, a new member of the tubulin superfamily encoded by *mipA* gene of *Aspergillus nidulans*. *Nature* **338**, 662-664 (1989).

64. H. Aldaz, L. M. Rice, T. Stearns, D. A. Agard, Insights into microtubule nucleation from the crystal structure of human gamma-tubulin. *Nature* **435**, 523-527 (2005).

65. S. Doxsey, D. McCollum, W. Theurkauf, Centrosomes in cellular regulation. *Annual Review of Cell and Developmental Biology* **21**, 411-434 (2005).

66. G. Pereira, E. Schiebel, Centrosome-microtubule nucleation. *Journal of Cell Science* **110**, 295-300 (1997).

67. S. Konzack, P. E. Rischitor, C. Enke, R. Fischer, The role of the kinesin motor KipA in microtubule organization and polarized growth of *Aspergillus nidulans*. *Molecular Biology of the Cell* **16**, 497-506 (2005).

68. B. Sheeman, P. Carvalho, I. Sagot, J. Geiser, D. Kho, Determinants of *S. cerevisiae* dynein localization and activation: implications for the mechanism of spindle positioning. *Current Biology* **13**, 364-372 (2003).

69. H. Maekawa, E. Schiebel, Cdk1-Clb4 controls the interaction of astral microtubule plus ends with subdomains of the daughter cell cortex. *Genes and Development* **18**, 1709-1724 (2004).

70. X. Lin, C. Momany, M. Momany, SwoHp, a nucleoside diphosphate kinase, is essential in *Aspergillus nidulans*. *Eukaryotic Cell* **2**, 1169-1177 (2003).

71. X. Lin, M. Momany, The *Aspergillus nidulans* swoC1 mutant shows defects in growth and development. *Genetics* **165**, 543-554 (2003).

72. M. Momany, P. J. Westfall, G. Abramowsky, *Aspergillus nidulans swo* mutants show defects in polarity establishment, polarity maintenance and hyphal morphogenesis. *Genetics* **151**, 557-567 (1999).

73. B. D. Shaw, C. Momany, M. Momany, *Aspergillus nidulans swoF* encodes an N-myristoyl transferase. *Eukaryotic Cell* **1**, 241-248 (2002).

74. B. D. Shaw, M. Momany, *Aspergillus nidulans* polarity mutant *swoA* is complemented by protein O-mannosyltransferase *pmtA*. *Fungal Genetics and Biology* **37**, 263-270 (2002).

75. S. Torralba, M. Raudaskoski, A. M. Pedregosa, F. Laborda, Effect of cytochalasin A on apical growth, actin cytoskeleton organization and enzyme secretion in *Aspergillus nidulans*. *Microbiology* **144**, 45-53 (1998).

76. S. Upadhyay, B. D. Shaw, A phosphoglucose isomerase mutant in *Aspergillus nidulans* is defective in hyphal polarity and conidiation. *Fungal Genetics and Biology* **43**, 739-751 (2006).

77. S. G. W. Kaminskyj, Fundamentals of growth, storage, genetics and microscopy in *Aspergillus nidulans*. *Fungal Genetics Newsletter* **48**, 25-31 (2001).

78. J. McCharen, B. D. Shaw. Generation of *Aspergillus nidulans* mutant collection via UV mutagenisis. *Unpublished work* (2004).

79. N. Osherov, J. Mathew, G. S. May, Polarity-defective mutants of *Aspergillus nidulans*. *Fungal Genetics and Biology* **31**, 181-188 (2000).

80. D. Chung, S. Upadhyay, B. Bomer, H. H. Wilkinson, D. J. Ebbole, B. D. Shaw, *Neurospora crassa* ASM-1 complements the conidiation defect in a *stuA* mutant of *Aspergillus nidulans*. *Mycologia* **107**, 298-306 (2015).

81. A. J. Clutterbuck, The validity of the *Aspergillus nidulans* linkage Map. *Fungal Genetics and Biology* **21**, 267-277 (2007).

82. P. C. Hickey, D. Jacobson, N. D. Read, N. L. Glass, Live-cell imaging of vegetative hyphal fusion in *Neurospora crassa*. *Fungal Genetics and Biology* **37**, 109-119 (2002).

83. A. Aleksenko, A. J. Clutterbuck, Autonomous plasmid replication in *Aspergillus nidulans*: AMA1 and MATE elements. *Fungal Genetics and Biology* **21**, 373-387 (1997).

84. E. C. Oakley, H. Edgerton-Morgan, B. R. Oakley, Tools for manipulation of secondary metabolism pathways: rapid promoter replacements and gene deletions in *Aspergillus nidulans*. in *Fungal Secondary Metabolism: Methods and Protocols,* N. P. Keller, G. Turner, Eds., Humana Press, New York, 143-161 (2012).

85. J. Sambrook, D. W. Russell, *Molecular Cloning: A Laboratory Manual* **3**, A. Irwin, Ed., Cold Spring Harbor Laboratory Press, New York (2001).

86. S. F. Altschul, W. Gish, W. Miller, E. W. Myers, D. J. Lipman, Basic local alignment search tool. *Journal of Molecular Biology* **215**, 403-410 (1990).

87. S. Aronov, mRNAs encoding polarity and exocytosis factors are cotransported with the cortical endoplasmic reticulum to the incipient bud in *Saccharomyces cerevisiae*. *Molecular Cell Biology* **27**, 3441-3455 (2007).

88. N. Takeshita, A. Ohta, H. Horiuchi, CsmA, a class V chitin synthase with a myosin motor-like domain, is localized through direct interaction with the actin cytoskeleton in *Aspergillus nidulans*. *Molecular Biology of the Cell* **16**, 1961-1970 (2005).

89. M. Tsuizaki, N. Takeshita, A. Ohta, H. Horiuchi, Myosin motor-like domain of the class VI chitin synthase CsmB is essential to its functions in *Aspergillus nidulans*. *Bioscience, Biotechnology, and Biochemistry* **73**, 1163-1167 (2009).

90. S. Treitschke, G. Doehlemann, M. Schuster, G. Steinberg, The myosin motor domain of fungal chitin synthase V is dispensable for vesicle motility but required for virulence of the maize pathogen *Ustilago maydis*. *The Plant Cell* **22**, 2476-2494 (2010).

91. S. A. Kuznetsov, D. T. Rivera, F. F. Severin, D. G. Weiss, G. M. Langford, Movement of axoplasmic organelles on actin filaments from skeletal muscle. *Cell Motility and the Cytoskeleton* **28**, 231-242 (1994).

92. J. S. Tabb, B. J. Molyneaux, D. L. Cohen, S. A. Kuznetsov, G. M. Langford, Transport of ER vesicles on actin filaments in neurons by myosin V. *Journal of Cell Science* **111**, 3221-3234 (1998).

93. H. Lodish, A. Berk, S. L. Zipursky, P. Matsudaira, D. Baltimore, J. Darnell, Section 7.2 Constructing DNA Libraries with λ Phage and Other Cloning Vectors. in *Molecular Cell Biology* **4**, W. H. Freeman, New York, 176-188 (2000).